Progetto S3 – Scenari di scuotimento in aree di interesse prioritario e/o strategico

Responsabili: Francesca Pacor (INGV-MI) e Marco Mucciarelli (Unibas)

TASK 3 – MOLISE - DELIVERABLE D7 VALIDATION SHAKING SCENARIOS

A cura di

UR1 – *Gianlorenzo Franceschina, Francesca Pacor, Dino Bindi, Lucia Luzi*
UR2 - *Giovanna Cultrera, Laura Scognamiglio*
UR9 – *Paola Morasca, Francesca Zolezzi*
UR10 – *Antonio Emolo, Frantisek Gallovic*

Luglio 2007

INDEX

1.   INTRODUCTION

The main goal of this report is the computation of the bedrock seismic motion at 5 municipalities located in the Molise area (Bonefro, S.Giuliano, Colletorto, S.Croce di Magliano, Ripabottoni, hereafter referred to as sites BNF, SGI, CLT, SCM and RPB, respectively). This area represents one of the validation case studies, planned in the framework of Project S3 which aim is the production of ground shaking scenarios for moderate magnitude earthquakes. Indeed, the recently occurred Molise earthquake represents a proper opportunity to compare synthetic simulations with real data. Acceleration time series were recorded during the October 31, 2002 and November 1, 2002 main shocks by analog and digital instruments managed by the Italian Civil Protection Department [DPC-SSN, 2004] while acceleration and velocity records were collected during the first month of seismic activity by DPC, INGV, INOGS, Dip.Te.Ris.(Genoa) (see §2.1 and Deliverable D6). Both strong and weak motion data were employed to infer regional ground motion prediction equations and spectral attenuation models (§2.3 and §2.4) while acceleration time series recorded during the first main shock by nearby stations were used to constrain the seismogenic sources of the October 31 and November 1, 2002 twin earthquakes (§4.1).

Bedrock shaking scenarios at different level of complexity were produced by ground motion prediction equations (scenarios of level 0, §4.2), high frequency (f>1Hz) simulations (scenarios of level I, §4.3) and broad band (0-12 Hz) simulations (scenarios of level II, §4.4). Comparison of results obtained with different simulations methods confirms the complexity of the Molise area as regard to both seismogenic and attenuation properties of the crust. Especially for this area the ground motion prediction is constrained by the demand of simulations reproducing different features of the seismic wavefield. In particular, the input motion for site effect modelling, performed at sites located in the epicentral area, was computed with a broad band technique able to reproduce the complete wave field in the frequency band 0-10 Hz in terms of acceleration time series (scenarios of level II scenarios).

2.   THE 2002 SEISMIC SEQUENCE

The October 31 (10:32 UTC) and November 1 (15:08 UTC), 2002, earthquakes (Mw=5.8 and Mw=5.7, respectively) struck the Molise area region killing young human lives in a school collapse and causing moderate damage in an area comprising 29 municipalities [Maffei and Bazzurro, 2004; Nuti et al., 2004]. Main shocks sources were located at about 20 km depth, on a deep seismogenic structure underlying the Apulia Platform [Valensise et al., 2004]. Seismicity was detected at corresponding depths by a temporary seismic network, installed soon after the first main event [Chiarabba et al., 2005]. More than 1900 aftershocks, located with errors lower than 0.5 km, revealed an east-west-trending nearly vertical buried structure extending from 10 to 25 km depth composed of two 15 km long main segments. For this twin earthquake, two different couples of seismogenic sources were proposed.
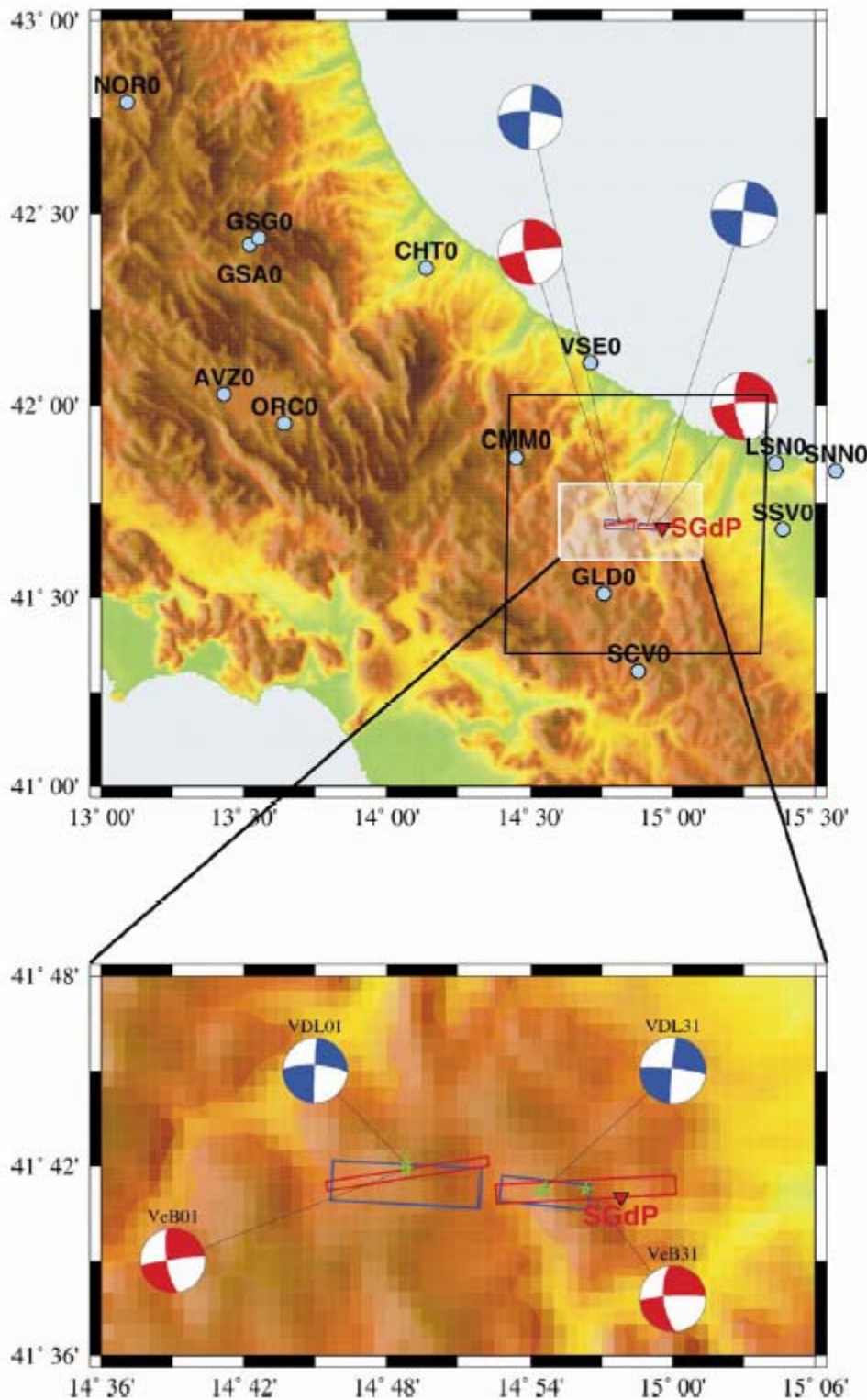
Figure 1. Surface projections and focal mechanisms of the fault models suggested for the October 31 and November 1, 2002 Molise earthquakes (lower panel). Red and blue symbols indicate the models of Basili and Vannoli [2005] and Valleè and Di Luccio [2005], respectively. Locations of the accelerometric stations recording the main events are also shown in the upper panel (black labels). The red label indicate the position of S.Giuliano di Puglia.

Based on inversion of teleseismic, regional and local seismic signals, Vallée and Di Luccio [2005] modelled the first event by a 5.2 x 14.2 km² fault plane extending from 6.0 to 20.1 km depth, and the second one by a 8.6 x 9.7 km² fault with depths ranging from 9.0 to 18.4 km. A fault model based on seismotectonic data [Basili and Vannoli, 2005] hypothesizes a similar fault for this second shock. However, this model associates the first event with a 10.5 x 8.0 km² fault extending from 12 to 19.9 km depth. Hereafter, we denote as VDL31, BV31, VDL01 and BV01 the fault models of Vallée and Di Luccio [2005] and Basili and Vannoli [2005] for the October, 31 and November, 1, 2002, earthquakes, respectively. Figure 1 shows the surface projections of these faults, with the location of accelerometric stations recording the main events. In this report, acceleration data recorded at hypocentral distances less then 60 km are employed to select the source model.

2.1.   Dataset

The data set exploited for deriving the ground motion models and for calibrating a spectral model of the quality factor Q(f) is composed by both strong motion (accelerometric) and seismic (velocimetric) recordings. The strong motion data set is composed by 195 recordings from 51 earthquakes in the local magnitude range 2.5-5.4 recorded by 29 accelerometers [DPC-SSN, 2004]. The recording sites are mostly installed on rock and stiff sites and the hypocentral distance of most recordings is less than 50km. The mainshocks have been mainly recorded by analog instruments of the national accelerometric network, while the temporary network was entirely composed of digital instruments that recorded the aftershocks.

The velocimetric data set is composed by 2895 recordings coming from 78 earthquakes recorded by 22 stations at hypocentral distances less than 50km.

The strong motion data obtained by analog instruments have been corrected for the baseline and instrument response and filtered in the average band-pass (0.5-20 Hz) in order to remove the low frequency noise, after a visual inspection of the Fourier amplitude spectra. The digital records have been corrected in order to remove the baseline and band-pass filtered in the average range (0.2-30 Hz). The sampling rate of the records is 200 Hz. The velocimetric data have been corrected for the instrument response and band pass filtered in the average range (0.5-25 Hz). The sampling rate is 100 Hz.

The recording sites have been classified according to the local lithology, in order to account for amplification effects. According to the available information only two classes can be distinguished, namely rock (Vs > 800 m/s) and soil (Vs < 800 m/s). The distribution of the events, the location of the temporary velocimetric stations and the accelerometric stations is shown in Figure 2, while Table 1 lists the characteristics of the velocimetric and accelerometric stations.
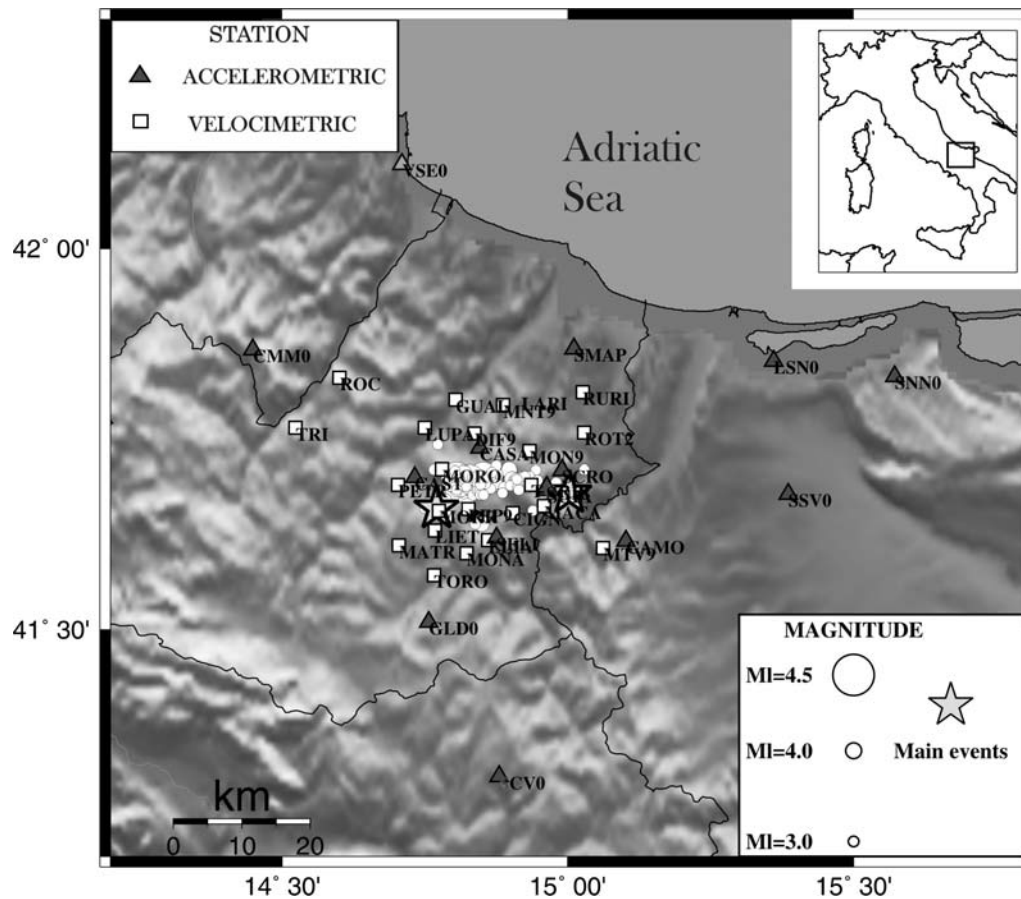
Figure 2. Distribution of the events, location of the temporary velocimetric and accelerometric stations.

2.2. Local magnitude

The velocimetric waveforms have been used to calibrate a local magnitude (ML) scale using synthetic Wood-Anderson amplitudes obtained from the horizontal components. The ML scale [Richter, 1935] has been calibrated following the parametric approach of Bakun and Joyner [1984]:

$$M_L = \log A + n \log(R/17) + k(R-17) + 2 - S \qquad (1)$$

where A is the observed maximum Wood-Anderson amplitude, n and k are attenuation coefficients, S is a station correction, and R is the hypocentral distance. In the calibration procedure, n has been set to 1 and the sum of the station corrections was set to zero. The magnitude has been calibrated using a sub-set of 572 recordings from 16 stations. The calibrated scale is characterized by a value of k equal to 0.0308. The station corrections range between -0.34 and 0.55, showing a good agreement with the local amplification effects estimated by computing the H/V spectral ratios (large positive magnitude corrections have been found for stations characterized by significant site amplification within the Wood-Anderson frequency band). Large standard deviation (up to 0.11 magnitude unit) have been obtained for stations that recorded few earthquakes. Finally, the obtained magnitudes range between 1.5 and 5.2. The recalculated magnitudes have been used to characterise all the events

recorded by the velocimetric stations.

Different choices were made to characterise the 51 events recorded by the accelerometric network. The localisation and moment magnitude determined by Chiarabba et al. [2005] were used for the 2 mainshocks, the recalculated magnitudes were assigned to the 35 events common to the velocimetric data set, while the localisation and magnitudes of the INGV bulletin were used to qualify the 16 events of the sequence occurred after the removal of the velocimetric network.

Table 1. Characteristics of the recording stations.

Name	Code	Latitude	Longitude	Site	type	Recorder	Sensor	Network
S.Elia a Pianisi	CIGN	41.654	14.904	R	d	LE5800	Lennartz5s	OGS mobile
Casacalenda	DIF9	41.758	14.837	S	d	LE5800	Lennartz5s	INGV mobile
S.Elia a Pianisi	ELIA	41.618	14.861	S	d	Mars	Lennartz5s	DipTeRis mobile
Guardalfiera	GUAL	41.802	14.804	S	d	Mars	Lennartz5s	DipTeRis mobile
Campolieto	LIET	41.631	14.768	S	d	Mars	Lennartz5s	DipTeRis mobile
Lupara	LUPA	41.765	14.750	S	d	Mars	Lennartz5s	DipTeRismobile
ColleTorto	MACA	41.663	14.959	R	d	Reftek-72A	CMG40T	INGV mobile
Matrice	MATR	41.611	14.705	S	d	Orion	Lennartz1s	OGS mobile
Larino	MNT9	41.795	14.887	R	d	LE5800	Lennartz5s	INGV mobile
Monacilioni	MONA	41.601	14.823	S	d	Marslite	Lennartz1s	OGS mobile
Montelongo	MON9	41.735	14.933	S	d	LE5800	Lennartz5s	INGV mobile
Morrone del Sannio	MORO	41.711	14.780	S	d	Mars	Lennartz5s	DipTeRis mobile
Morrone del Sannio	MORR	41.657	14.775	S	d	Reftek-72A	Lennartz5s	INGV mobile
Monte Rotaro	MTV9	41.608	15.062	S	d	Orion	Lennartz1s	INGV mobile
Ripabottoni	PEP9	41.659	14.826	S	d	LE5800	Lennartz5s	INGV mobile
Putrella	PETR	41.691	14.703	R	d	Mars	Lennartz5s	DipTeRis mobile
Roccavivara	ROC	41.831	14.601	S	d	Marslite	Lennartz1s	OGS mobile
Rotello	ROT2	41.759	15.029	S	d	Reftek-130	CMG40T	INGV mobile
Ururi	RURI	41.812	15.026	R	d	Reftek-130	CMG40T	INGV mobile
Toro	TORO	41.572	14.766	R	d	Mars	Lennartz5s	DipTeRis mobile
Bonefro	TORR	41.691	14.936	S	d	Reftek-72A	CMG40T	INGV mobile
Triveneto	TRI	41.765	14.524	S	d	Orion	Lennartz1s	OGS mobile
Cast. Messer Marino	CMM0	41.868	14.449	R	d	Altus Etna	Episensor	RAN
S. Marco dei Cavoti	SCV0	41.306	14.88	S	d	Altus Etna	Episensor	RAN
Gildone	GLD0	41.51	14.757	S	a	Teledyne RFT250		RAN
Sannicandro Garg.	SNN0	41.833	15.572	R	a	SMA1		RAN
San Severo	SSV0	41.679	15.386	S	a	SMA1		RAN
Vasto Europa	VSE0	42.111	14.71	S	a	Teledyne RFT250		RAN
Lesina	LSN0	41.853	15.36	S	a	SMA1		RAN
Casalnuovo M.	CAMO	41.617	15.102	S	d	Altus Etna	Episensor	RAN mobile
Casacalenda	CASA	41.739	14.846	S	d	Altus Etna	Episensor	RAN mobile
Castellino del B.	CAST	41.701	14.732	S	d	Altus Etna	Episensor	RAN mobile
Larino	LARI	41.805	14.919	R	d	Altus Etna	Episensor	RAN mobile
Santa Croce di M.	SCRO	41.71	14.99	S	d	Altus Etna	Episensor	RAN mobile
S. Elia a Pianisi	SELI	41.621	14.875	R	d	Altus Etna	Episensor	RAN mobile
S. Giuliano di P. (A)	SGIA	41.684	14.964	R	d	AltusEverest	Episensor	RAN mobile
S. Giuliano di P. (B)	SGIB	41.688	14.963	S	d	AltusEverest	Episensor	RAN mobile
S. Martino in P.	SMAP	41.869	15.011	S	d	Altus Etna	Episensor	RAN mobile

2.3. Ground Motion Prediction Equations (GMPE)

The attenuation relationships are calibrated considering the following ground-motion model:

$$\log_{10} Y = a + bM + c \log_{10} R + s_{1,2} + \sigma \qquad (2)$$

where Y is the derivative variable, M is the local magnitude, R is the hypocentral distance (in km), σ is the standard deviation of the logarithm of the derivative variable. We calibrated model (2) for peak ground acceleration (PGA) and peak ground velocity (PGV). The models are derived for both the maximum horizontal (H) and vertical (V) components. The PGA is expressed in unit of g while PGV is measured in cm/s. The ground motion model (2) accounts for the site classification through the site coefficients $s_{1,2}$. The coefficients a, b, c, d and $s_{1,2}$ are determined by applying the random effects model [Abrahamson and Youngs, 1992] that allows the determination of the inter-event, inter-station, and record-to-record components of variance [e.g, Bindi et al., 2006]. In particular, the coefficient s1 for the rock site is constrained to zero. In totality 886 records were selected, recorded by 37 stations in the hypocentral distance range from 10 to 50 km. The magnitude-distance distribution of the records is shown in Figure 3. The acceleration data sample a wider range of magnitude and distances, while, on the contrary, almost the totality of velocimetric data have been recorded at hypocentral distances between 20 and 30km.
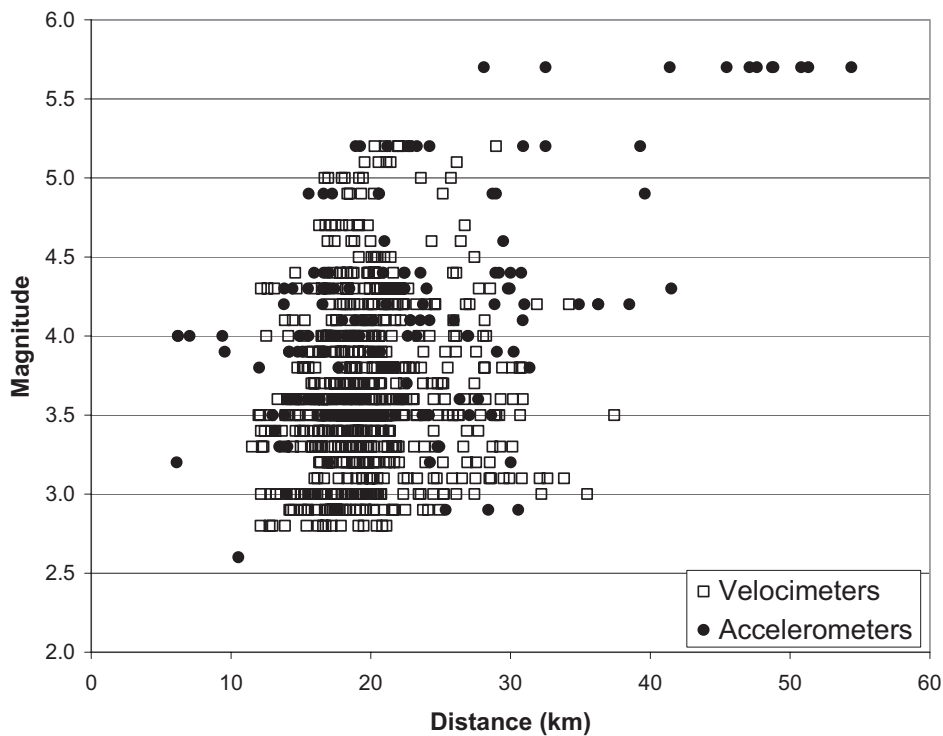

Figure 3. Magnitude-distance distribution of the records used for the regression.

The coefficients of equation (2) are listed in Table 2 and Table 3, which refers to the intra-event and intra-station analysis, respectively. The total standard deviation is mainly determined by the record-to-record variability. In particular, the intra-event distribution of error shows that the calibrated local magnitudes and the bulletin ones provide errors of comparable size.

Figure 4 shows the PGA and PGV attenuation curves for local magnitude 4.4 and soil sites, together with the observed velocimetric and accelerometric data. Data obtained by different sensors demonstrate an acceptable agreement.

Figure 5a shows that horizontal and vertical components are similar in attenuation pattern but not in amplitude, and a dependence on magnitude can be observed. Figure 5b points out the importance of distinguishing soil classes.

Table 2. Regression coefficients to detect the sigma intra-event (HPHA = horizontal PGA; VPGA = vertical PGA; HPGV = vertical PGV; VPGV = vertical PGV)

	a	b	c	s	s1	σ_eve	σ_rec	σ_tot
HPGA								
	-4.417	0.770	-1.097	0	0.123	0.069	0.339	0.345
VPGA								
	-4.128	0.722	-1.250	0	0.096	0.085	0.338	0.348
HPGV								
	-3.186	0.902	-1.317	0	0.155	0.085	0.312	0.323
VPGV								
	-3.039	0.836	-1.408	0	0.100	0.109	0.283	0.303

Table 3. Same as Table 2 but for the sigma intra-station.

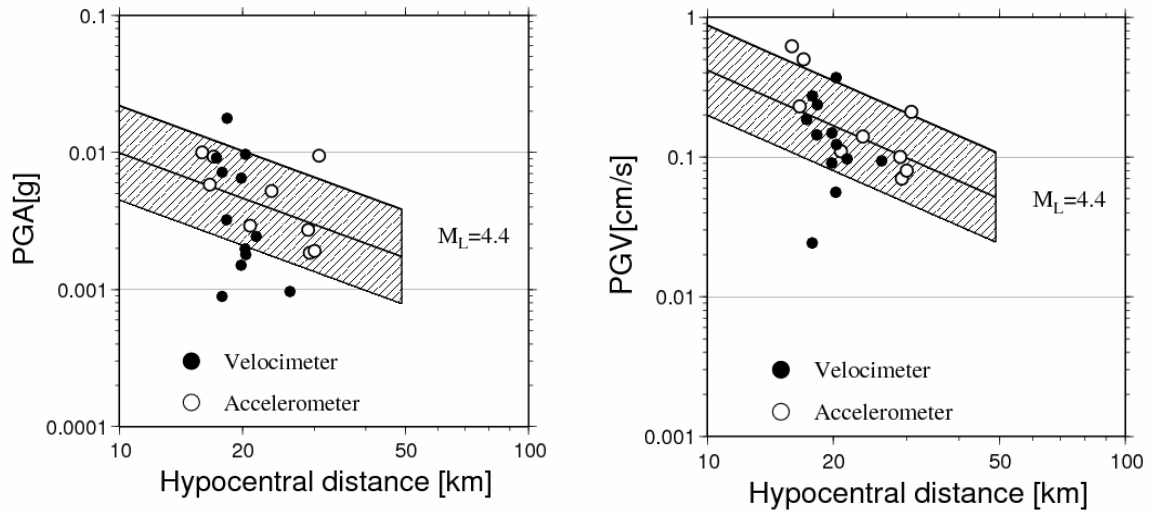|	a	b	c	s	s1	σ_sta	σ_rec	σ_tot
HPGA								
	-4.367	0.774	-1.146	0	0.119	0.077	0.337	0.346
VPGA								
	-4.066	0.729	-1.322	0	0.090	0.105	0.335	0.351
HPGV								
	-3.129	0.905	-1.373	0	0.151	0.086	0.313	0.325
VPGV								
	-2.988	0.839	-1.460	0	0.094	0.096	0.289	0.305

Figure 4. PGA and PGV Attenuation curves for soil sites (Ml = 4.4). Black and white dots represent observed data.

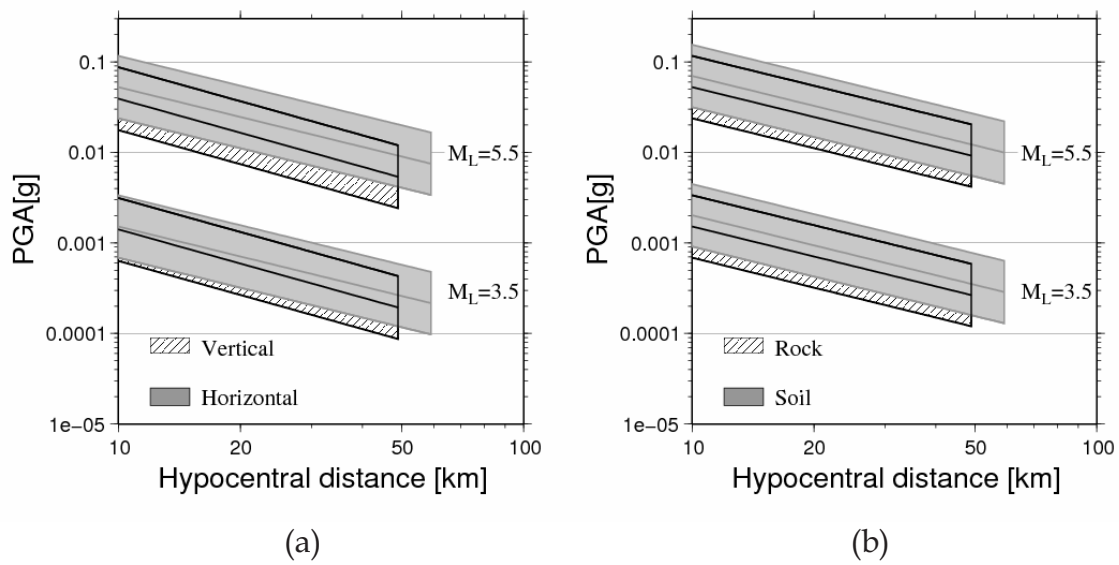(a)   (b)

Figure 5. Horizontal and vertical PGA for rock sites (a); horizontal PGA attenuation curves for rock and soil sites (b)

2.4. Spectral attenuation

The attenuation with distance is determined by applying the generalized spectral inversion (e.g., Castro et al., 1990). The velocity spectrum $U(f,r_{ij})$ at frequency f of event j recorded at station i is modeled as

$$U(f,r_{ij}) = \frac{1}{r_{ij}} \exp\left(-\frac{\pi f r_{ij}}{Q(f)\beta}\right)\hat{S}_j(f) \tag{3}$$

where r_{ij} is the hypocentral distance, $\hat{S}_j(f)$ is a scalar depending upon the spectral amplitude of source j, $Q(f)$ is the quality factor and β the average shear wave velocity (in this work fixed to 3.5 km/s). The equation (3) implies that the geometric spreading exponent has been fixed to 1. First, $Q(f)$ is determined by numerically solving equation (3) and then it is described in terms of the model $Q(f)=Q_0 f^\alpha$, by performing a least-squares regression.

The quality factor is determined by composing the two horizontal components and computing the Fourier amplitude spectra of time windows having a duration of 5 s, starting from the S-wave arrival. The evaluation of $Q(f)$ is performed twice: in the first inversion, 879 recordings between 6 and 50 km are considered while, in the second inversion, 917 recordings with distances up to 200 km are handled. Anyway, most of the distances are around 20 km. For example, in the first inversion 88% of data are between 15 and 30 km.

Figure 6 shows the obtained $Q(f)$ models, described by the following equations:

$$Q(f) = \begin{cases} 37.67\, f^{1.22} & 1 \le f \le 8\,\text{Hz} \\ 476 & 8 < f \le 20\,\text{Hz} \end{cases} \tag{4}$$

$$Q(f) = \begin{cases} 11.26\, f^{1.43} & 1 \le f \le 8\,\text{Hz} \\ 218 & 8 < f \le 20\,\text{Hz} \end{cases} \tag{5}$$

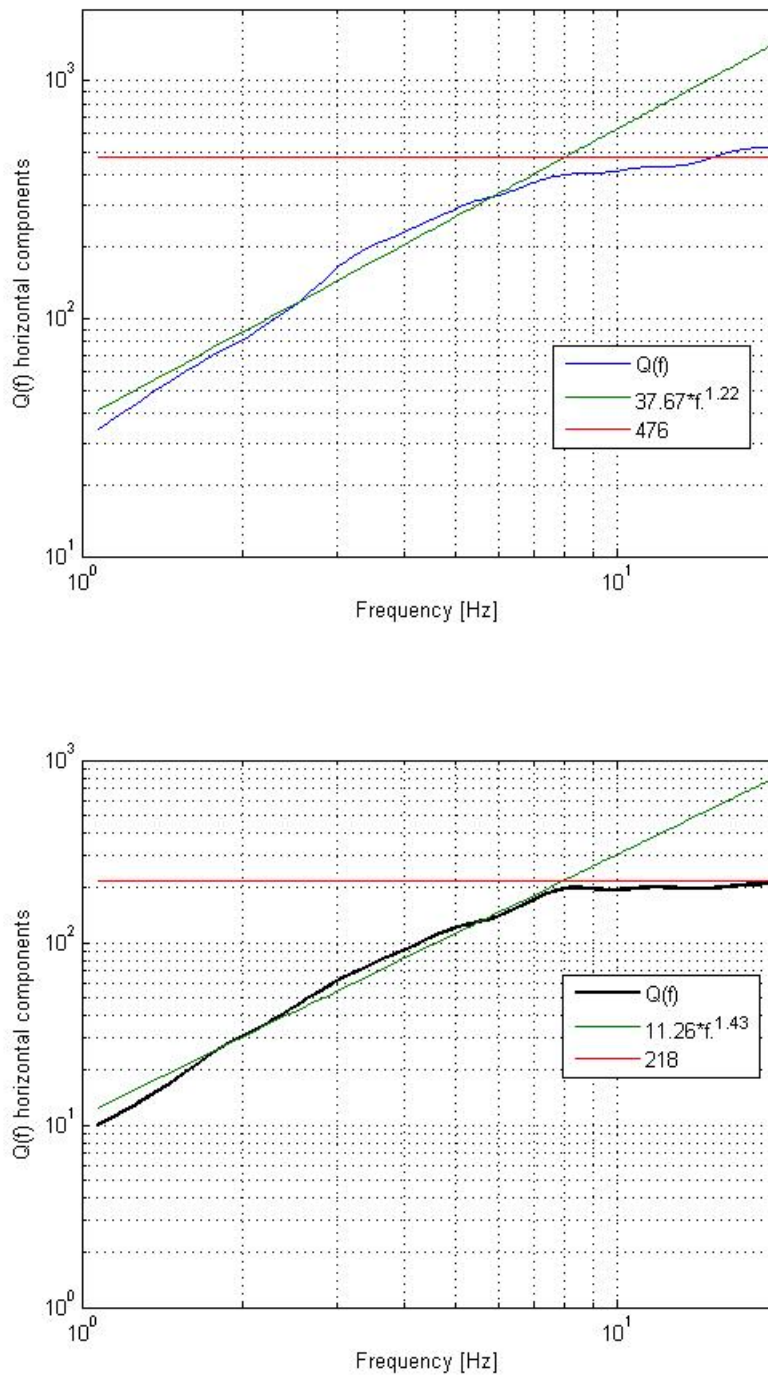where equation (4) is relevant to distance up to 200 km while equation (5) to distances smaller than 50 km.

Figure 6. Top: quality factor $Q(f)$ against frequency (black) and best fit $Q(f)=Q_0f^\alpha$ models (green and red) for distances up to 200 km (equation 4). Bottom: the same but for distances up to 50 km (equation 5).

3.   MODELLING METHODS

Different numerical methods have been adopted for simulating strong ground motion in the Molise area. For bedrock simulations, two hybrid stochastic-deterministic methods were used: the Deterministic-Stochastic Method of Pacor et al. [2005] (hereafter referred to as DSM), and the Hybrid Integral-Composite k-squared source model by Gallovic and Brokesova [2007] (hereafter referred to as HIC). These simulation techniques take into account finite fault effects considering a radial rupture propagation with constant rupture velocity and heterogeneous final slip distribution. Seismic waves are propagated through a crustal 1D velocity model. Spectral attenuation model is also taken into account. Both methods allow effective simulations although specifying only a relatively small number of input parameters, representing average properties of seismic source and waves propagation.

The DSM is a modification of the stochastic point source simulation method of Boore [2003], accounting for finite fault effects by a simplified formulation of the isochron theory [Bernard and Madariaga, 1984; Spudich and Frazer, 1984].

Schematically, the synthesis of a time series consists of:
- A) Computation of the Deterministic Acceleration Envelope (DAE) of shear waves radiated from an extended fault.
- B) Generation of the white noise time-sequence.
- C) Windowing of the noise sequence with the DAE.
- D) Transformation to the frequency-domain.
- E) Introduction of the point-source-like reference spectrum, that takes into account of finite fault properties of the source.
- F) Transformation back to the time domain.

Application of steps from A) to D) implies that the resulting acceleration time series involves stochastic properties of the adopted Gaussian white noise and deterministic properties of the acceleration envelopes and point-source-like reference spectra (obtained by means of the kinematic finite-fault source modelling). The method simulates only direct shear waves.

The HIC method combines the low-frequency and the high-frequency source modelling in order to obtain broad band time series based on the same hypothesis of slip distribution on the fault. In this model the faulting process is decomposed into slipping on individual, formal, overlapping subsources of various sizes, distributed randomly along the fault. A subsources database is first built, including the subsources' positions on the fault, their dimensions, mean slips (and consequently seismic moments) and corner frequencies. Subsource dimensions are taken as integer fractions of fault's length and width. Scaling properties of the subsources are the same as used by Zeng et al. [1994]. Their number-size distribution obeys a power law with fractal dimension D=2 and their mean slips are proportional to their dimensions (so-called constant stress-drop scaling). The subsources scaling implies that the subsources compose k-square slip distribution [Andrews, 1980]. Note that although such a decomposition is inherent to the composite approaches, in the employed hybrid model the same set of subsources is used both in the integral (low-frequency)

and composite (high-frequency) calculations. More specifically, in the low-frequency range, the computation is performed according to the well-known representation theorem. We discretize the fault densely enough to evaluate the representation integral correctly up to a certain frequency. The static slip at a point is given by the sum of static slips of all the subsources from the database that contain the point (assuming a k-squared slip distribution on each individual subsource). The rupture time is given by the distance of the point from the nucleation point assuming constant rupture velocity. The slip function is assumed to be a smoothed ramp with constant rise time. As regards the high-frequency range, the subsources from the database are treated as individual point sources with Brune's source time function [Brune, 1970]. Their seismic moments and corner frequencies are obtained directly from the database. The rupture time is given by the time the rupture needs to reach the subsource's center (assuming the same constant velocity as for the integral approach). In the cross-over frequency range we apply weighted averaging of the integral and composite parts of the spectrum. Let us emphasize that this approach provides particular frequency dependent directivity effect: while at low frequencies the wavefield is coherent due to evaluation of the representation integral, at high frequencies the wave-field contributions sum incoherently due to the random subsources positions and, therefore, the directivity effect vanishes. Moreover, following paper by Satoh [2002], in which the author shows that the radiation pattern vanishes at high frequencies, we simulate the vanishing radiation pattern by considering random variations of the focal mechanism (±90° for strike, dip and rake) prescribed for the individual point sources in the composite part of the computation. As such, the method can be combined with any technique yielding Green's functions. In this paper we utilize the discrete wave-numbers method [Bouchon, 1981]. For more detailed explanation of the hybrid modeling technique see Gallovic and Brokesova [2006].

An additional simulation technique (the Empirical Green Function method) was also employed in order to simulate the ground motion at sites where weak motion records were obtained during the 2002 sequence. Both method and results are presented in Deliverable D2.

4.   GROUND SHAKING SCENARIOS

Bedrock shaking scenarios were produced exploiting the possibility of comparison between the acceleration time series recorded during the October 31 main shock and synthetics. Indeed, accelerations recorded at nearby stations (hypocentral distances < 60 km), show high variability in both amplitude and duration (Figure 7 and Table 4), with PGAs ranging between 4.9 to 61.3 gal and durations (measured as the time interval during which the squared acceleration rises from 5 to 75% of its maximum value) between 4 and 20 s. As regard the directivity, the position of stations located eastward from the sources (namely LSN, SSV and SNN) and of stations located westward (CMM, GLD and VSE) is particularly relevant (see Figure 1). These are characterized by different soil categories but, unfortunately, two of them did not record both events. However, it is noteworthy that CMM and SNN, both classified as "Rock" and located at similar distances, recorded the first event with different levels of shaking (mean horizontal PGAs being 36.0 and 6.2 gal for SNN and CMM, respectively). Moreover, the second main shock produced PGA values at westward sites (particularly CMM and GLD) comparable to the first shock but lower values at SSV (mean horizontal PGAs being 54.1 and 22.7 gal for the first and the second shock, respectively).

At a first stage, the DSM was employed to investigate the supposed directivity effects with the aim of defining the most plausible couple of seismogenic sources for the October 31 and November 1 main shocks. Comparison of acceleration data recorded at nearby stations with synthetics obtained by the DSM, performed in terms of frequency content and peak ground accelerations, allowed choosing both source geometry and rupture mechanism. Attenuation properties were defined by the regional attenuation model inferred from acceleration and velocity data (§2.4).
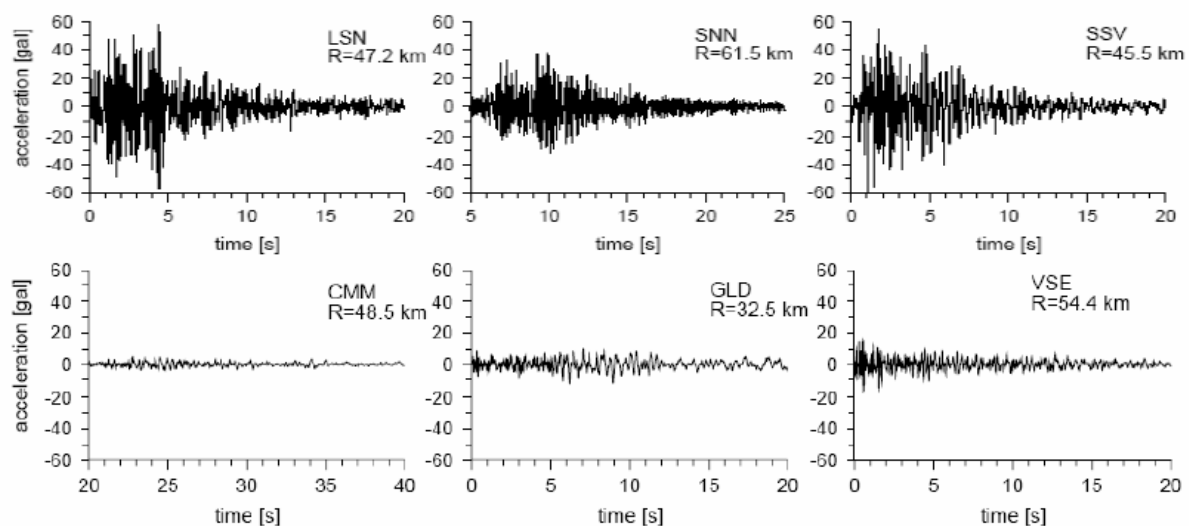

Figure 7. NS component acceleration time series recorded during the October 31, 2002 Molise earthquake at stations with hypocentral distance < 60 km. Stations LSN (Lesina), SNN (Sannicandro) and SSV (San Severo) are located eastward to the epicentre, stations CMM (Castiglione Messer Marino), GLD (Gildone) and VSE (Vasto Europa) are located westward.

Table 4. Acceleration data of the October 31 and November 1, 2002, Molise (Southern Italy) earthquakes. Soil: site geology according to the National Seismic Survey of Italy (SSN) classification; I: instrument type (A=analog, D=digital); R: hypocentral distance according to Chiarabba et al., [2005]; pga [NS] and pga [EW] : corrected peak ground accelerations of North-South and East-West components, respectively; k and σ_k : mean diminution parameter and its standard deviation, respectively, estimated from horizontal components of recordings of the two October-November main shocks.

Code	Station name	Soil	I	October 31, 2002, M_W=5.8			November 1, 2002, M_W=5.7			k	σ_k
				R [km]	pga [NS] [gal]	pga[EW] [gal]	R [km]	pga [NS] [gal]	pga[EW] [gal]	[s]	[s]
AVZ	Avezzano	Stiff	D	130.4	6.7	3.7	122.9	3.2	3.7	0.1700	0.0024
CHT	Chieti	Soft	D	100.5	5.7	6.7	95.2	7.9	7.6	0.0775	0.0009
CMM	Castiglione M. Marino	Rock	D	48.5	4.9	7.9	41.3	5.6	7.0	0.0555	0.0006
GLD	Gildone	Stiff	A	32.5	12.1	17.6	28.1	17.1	18.3	0.0625	0.0014
GSA	Gran Sasso Assergi	Stiff	D	142.5	1.3	1.2	136.0	1.2	1.2	0.0580	0.0006
GSG	Gran Sasso Laboratorio	Rock	D	141.2	0.3	0.2	134.9	0.3	0.2	0.0517	0.0004
LSN	Lesina	Soft	A	47.2	58.4	62.1	-	-	-	0.0410	0.0013
NOR	Norcia	Stiff	D	194.5	1.4	1.8	188.5	1.0	1.6	0.1232	0.0027
ORC	Ortucchio	Rock	D	111.5	3.7	4.0	103.9	3.0	3.1	0.0700	0.0009
SCV	S. Marco dei Cavoti	Stiff	D	-	-	-	47.0	4.6	4.4	0.0695	0.0009
SSV	San Severo	Soft	A	45.5	61.3	47.8	50.8	25.7	20.0	0.0220	0.0013
SNN	Sannicandro Garganico	Rock	A	61.5	37.3	34.7	-	-	-	0.0330	0.0055
VSE	Vasto Europa	Stiff	A	54.4	17.6	42.0	51.3	15.6	33.4	0.0447	0.0021

Bedrock scenarios for extended areas were produced using GMPE (scenarios of level 0) and extended-fault high frequency simulations (scenarios of level I) for both the October 31 and November 1, 2002 events. Bedrock scenarios at specified sites located in the epicentral area (BNF, SGI, CLT, SCM and RPB) were produced by broad-band simulations (scenarios of level II).

After filtering between 1 and 12 Hz, the time series obtained at sites BNF, SGI, CLT, SCM and RPB (hypocentral distances < 20 km) by scenarios of level I and level II, were compared to each other in order to test the reliability of the computed input motion. Scenarios of level I and II were also compared to each other at sites SGI, GLD, SSV and CMM (hypocentral distances < 48 km) in terms of frequency content. Scenarios of level 0, I and II were also compared in terms of peak ground accelerations up to 150 km hypocentral distance.

4.1.   Validating predictive models

Table 5 summarizes the source parameters adopted for simulation of the October 31, 2002, event. We consider VDL31 and BV31 source geometries with nucleation points constrained by the epicenter location. As a consequence, only BV31 model implies WE unilateral rupture propagation. Seismic moment is inferred from the moment magnitude considered and average slips are computed assuming μ=3.6x10^{11} dyne/cm^{2}. Both models are compatible with Wells and Coppersmith [1994] relationships relating moment magnitude to rupture area.   A constant rupture velocity of 2.8 km/s (corresponding to 0.8V$_S$) is assumed in all simulations.

Table 5. Source parameters adopted for simulation of the October 31, 2002, Molise earthquake, according to Vallée and Di Luccio [2005] (VDL31) and Basili and Vannoli [2005] (BV31). M_W : moment magnitude; M0 : seismic moment ; Δu : average slip ; L and W : source dimentions; φ, δ and λ: strike, dip and rake; Z_{TOP} : top depth.

	M_W	$M_0[10^{17}Nm]$	Δu [cm]	L x W [km²]	φ[°]	δ[°]	λ[°]	Z_{TOP} [km]
VDL31	5.8	5.6	25	5.2 x 14.2	276	84	-177	6.0
BV31	5.8	5.6	20	10.5 x 8.0	267	82	-157	12.0
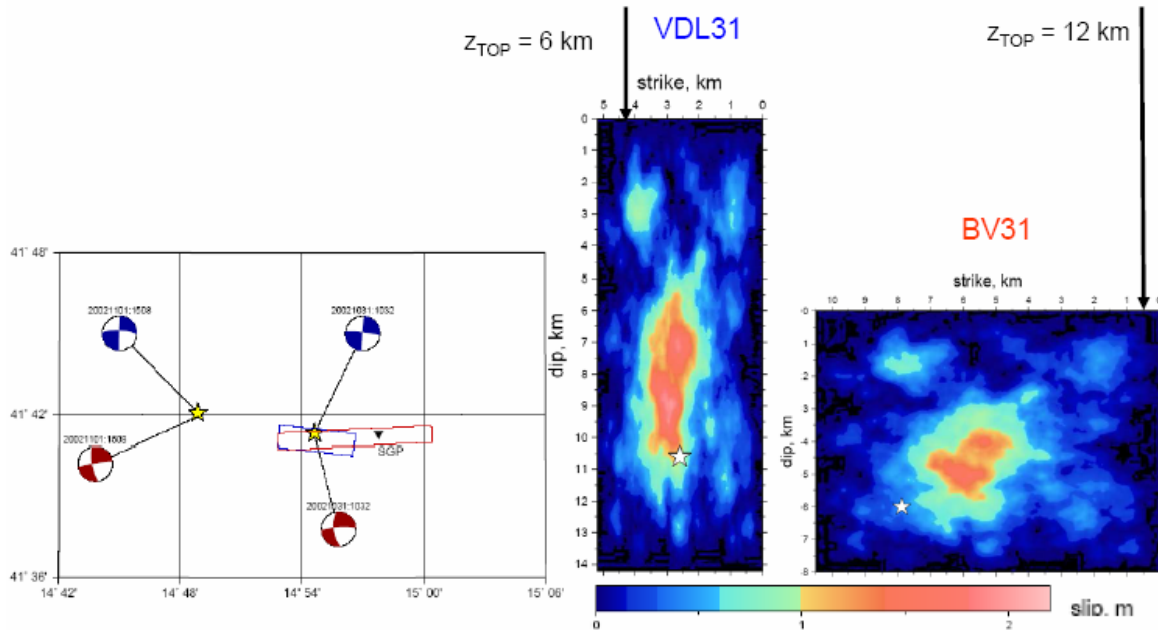
Figure 8. Fault surface projections (left) and slip distributions (right) adopted for the October 31, 2002, Molise main shock. Blue and red symbols represent VDL31 and BV31 fault models, respectively. Yellow star marks the surface projection of nucleation points corresponding to hypocenter locations (white stars on right panels).   Location and focal mechanisms of the November 1, 2002, and location of S.Giuliano di Puglia (SGP) are also shown.

Table 6. Crustal model used for finite fault simulations.

depth of layer [km]	Vp [km/s]	Vs [km/s]	ρ[g/cm³]	Qp	Qs
0.00	4.00	2.30	2.400	300.	150.
3.00	6.30	3.64	2.750	600.	300.
28.00	8.00	4.62	3.250	1000.	500.

For both models, k-square slip distributions are assumed. They come from the HIC model, i.e. from a random realization of the subsources distribution. To introduce an asperity in the center of the fault, the position of the largest subsources is imposed. Figure 8 shows the surface projections of the assumed faults and the adopted slip models. The crustal model (Table 6) is taken from Vallée and Di Luccio [2005]. The spectral attenuation model $A_P(\omega,R)$ involves $Q(f) = 37.7\, f^{1.2}$ (§2.4) and site dependent diminution parameter k, that is estimated using horizontal components recorded

during the October and November main events.   A suitable frequency band (depending on quality of data, generally ranging from 3-4 Hz to 20-25 Hz) was chosen in order to perform a reliable regression.

Figure 9 shows some examples of *k* estimates and Table 4 summarizes the results. The *k* estimates are generally characterized by low uncertainties (relative errors are of the order of a few percent). Except for SSV, the well-defined linear decay allows for stable regressions, generally independent of slight changes of the adopted frequency band. Combined effects of site amplification, anisotropic attenuation and directivity can be supposed to explain the observed differences between eastward and westward stations in the October/November 2002 Molise earthquakes. In order to consider a rough estimation of site effects at all the abovementioned sites, a computation of HVSRs was performed with acceleration data (Figure 10). Especially eastward stations show pronounced amplifications in specific frequency bandwidths, with amplitude ratios up to 10.
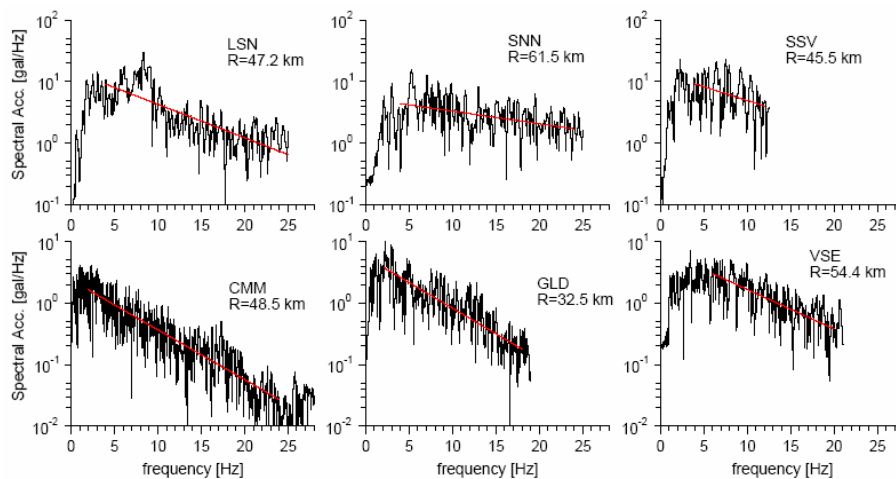
Figure 9. Estimates of *k* from acceleration NS components recorded during the October 31 main shock at stations CMM, GLD, VSE, LSN, SNN and SSV. Frequency bandwidths for regressions were chosen according to the corner frequency of the event and the high frequency noise of data.
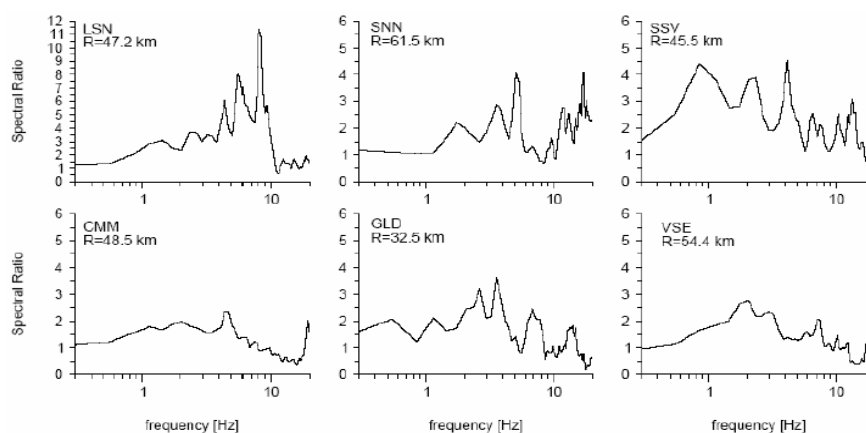

Figure 10. Mean value of the H/V spectral ratios estimated using acceleration data recorded during the October 31 and November 1 main shocks at stations CMM, GLD, VSE, LSN, SNN and SSV.

Comparison of synthetic and recorded acceleration amplitude Fourier spectra at nearby stations (hypocentral distance < 60 km) is shown in Figure 11 for DSM simulations. Site effects were introduced by dividing the recorded acceleration spectra with the H/V spectral ratios of Figure 10. Notwithstanding the amplification shown by some of the stations in specific frequency bands, the eastward sites (LSN, SNN, SSV) are generally characterized by higher spectral levels with respect to the westward ones (GLD, CMM, VSE). Since high frequency spectral level obtained through DSM simulations depends on the corner frequency squared, eastward sites show higher synthetic spectral accelerations than westward sites when BV31 model is adopted. Especially for eastward sites, BV31 model produces a better fit with recorded data than VDL31 model.

Acceleration spectra recorded at westward sites are also better fitted with the BV31 model, even if with a lower level of confidence. The model bias was computed in terms of RMS between simulated and observed spectral amplitudes. Except for VSE, we obtained RMS values less and greater then 0.4 for models BV31 and VDL31, respectively. It is noticeable that VSE distance and back-azimuth involve identical DSM simulations with VDL31 and BV31 models. PGAs simulated by DSM are compared with recorded PGAs in Table 7. Stations GLD, SSV and SSN show the best agreement between recorded and synthetic data obtained by BV31 model. For the other stations synthetic data do not fit the observed peaks so well. However, BV31 model still shows a better fit than VDL31 model. Global comparison of DSM simulations with acceleration data recorded at nearby stations thus favours a unilateral propagation of the rupture of the October 31, 2002 main shock.
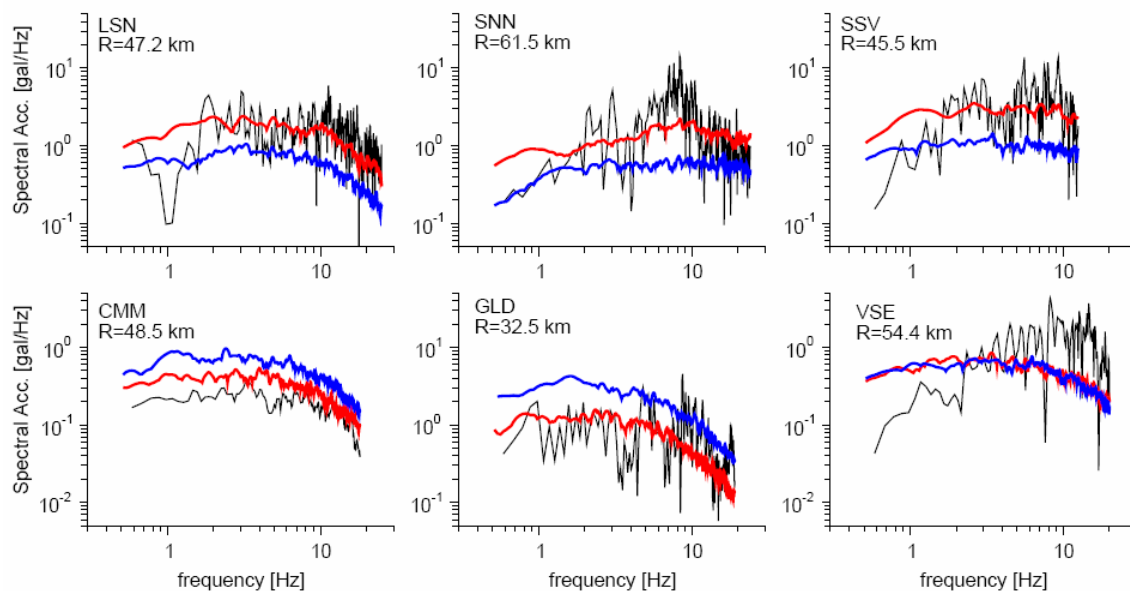

Figure 11. Comparison between DSM synthetic (coloured lines) and recorded (black lines) acceleration spectra of the October 1 main event (NS components) at stations CMM, GLD, VSE, LSN, SNN and SSV. Blue and red lines refer to VDL31 and BV31 models, respectively. Site effects were taken into account by dividing the recoded spectra with H/V spectral ratios of Figure 10.

Table 7. PGAs obtained by DSM simulations with BV31 and VDL31 models compared with recorded PGAs at nearby stations. R: hypocentral distance according to Chiarabba et al., [2005]; pga [EW], pga [NS] and pga[MH]: recorded and simulated peak ground accelerations of East-West, North-South and Mean Horizontal components, respectively. The model bias between synthetic (As) and observed (Ao) acceleration spectra is reported in the last two columns for BV31 and VDL31 models, respectively.

Code	Station name	Distance	Acceleration data			BV31	VDL31	BV31	VDL31
		R [km]	pga [EW] [gal]	pga [NS] [gal]	pga[MH] [gal]	pga[MH] [gal]	pga[MH] [gal]	RMS (Log As – Log Ao)	RMS (Log As – Log Ao)
CMM	Castiglione M. Marino	48.5	7.9	4.9	6.2	5.4	8.1	0.23	0.45
GLD	Gildone	32.5	17.6	12.1	14.6	11.5	31.8	0.23	0.50
LSN	Lesina	47.2	62.1	58.4	60.2	36.5	13.0	0.30	0.39
SSV	San Severo	45.5	47.8	61.3	54.1	63.7	17.1	0.26	0.41
SNN	Sannicandro Garganico	61.5	34.7	37.3	36.0	46.9	16.1	0.37	0.45
VSE	Vasto Europa	54.4	42.0	17.6	27.2	10.0	8.1	0.47	0.46

4.2. Level 0: scenarios from GMPE

Ground shaking scenarios in terms of PGA as a function of distance were produced by different GMPE available for the area. The regional empirical equation presented in §2.3 was obtained with data characterized by hypocentral distances in the range 10-50 km and magnitudes in the range 2.8-5.7, with more than 95% of data coming from events with magnitude < 5.3. In addition to this equation we thus consider the empirical relationship developed by Sabetta and Pugliese [1996] for the whole national territory (hereafter referred to as SP96), together with the Ambraseys [1995] relation, valid for Europe (hereafter referred to as A95). The main advantages of the latter are the large amount of acceleration data employed for the analysis (more then 1600 records from 865 events), the range of magnitude (3<Ms<7.3) and the relatively large number of data of deep events (about 40 percent of data has hypocentral depth > 14 km). Indeed, due to the high depth of the event, it is important to employ depth-controlled empirical relationships to provide seismic scenarios for the epicentral area of the Molise earthquake.

Figure 12 shows the horizontal PGA as a function of fault distance (f_d) predicted for the October 31 main shock by the abovementioned empirical equations. Far from the source (f_d > 10 km), both SP96 and A95 predict similar values of PGA, with the larger dispersion presented by A95. Instead, for f_d < 10 km, the depth-controlled relationship (A95) underestimates the peak values predicted by SP96.

Equation (2) can be adopted in a narrow range of distances. It presents the largest dispersion and underestimates the PGA predicted by A95 of a factor 3 in the whole range of distances. It is noteworthy that the use of this relation as GMPE for the Molise earthquake is to consider with caution due to the small magnitudes characterizing the dataset employed for its derivation.
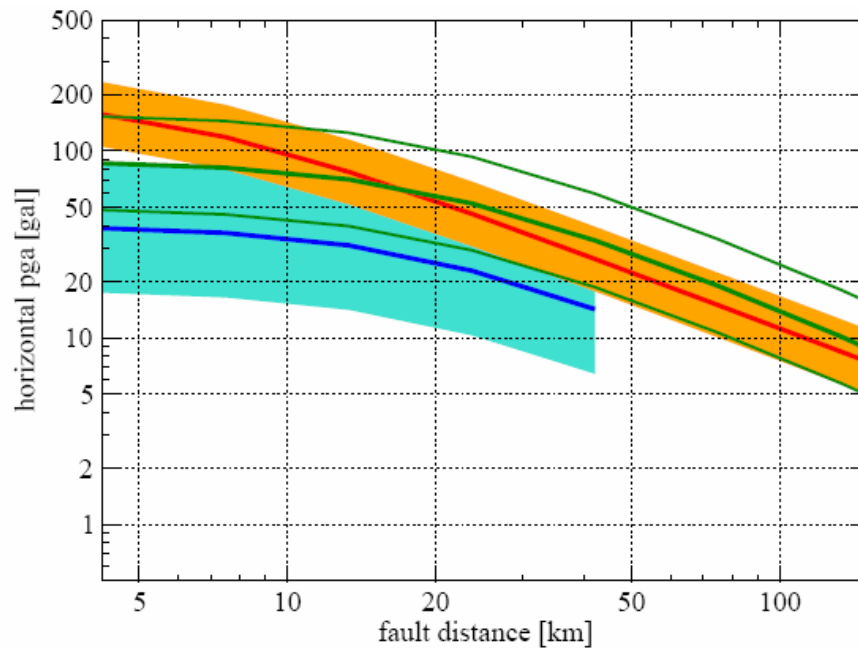
Figure 12. Horizontal PGA attenuation curves for rock sites predicted for the October 31, 2002 Molise earthquake by equation (2) (blue line); Sabetta and Pugliese [1996] (red line) and Ambraseys [1995] (thick green line). Shaded areas and thin green lines correspond to ±1std

4.3. Level I: DSM scenarios

Bedrock shaking scenarios have been computed by high frequency simulations (DSM) at grid points regularly spaced of 10 km up to 150 km epicentral distance for both the October 31 and November 1 main shocks. The source parameters adopted for simulations (Table 8) were inferred from Basili and Vannoli [2005] after comparison of synthetics with acceleration data recorded a nearby stations (§4.1).

Figure 13 shows the surface projections of the faults and the adopted k-squared slip distributions. A constant rupture velocity of 2.8 km/s (corresponding to $0.8V_S$) was assumed for both earthquakes. The crustal 1D model and the spectral attenuation models were assumed as in §4.1 considering $Q(f) = 37.7 \, f^{1.2}$, and a spectral decay parameter k of 0.02 s was employed for each site.

The mean component of the horizontal PGA obtained by averaging the results of 30 stochastic DSM simulations is shown in Figure 14 for the October 31 mainshock. As results of the hypothesized directivity, the maximum shaking area is located eastward respect to the surface projection of the fault. More then 100 gal PGA are reached in an area of about 400 square kilometres with maximum values around 160 gal. Due to the assumed fault depth, the areas characterised by the highest values of the ground motion do not show the usual elongated shapes. In this case, directivity effects only shift the position of the maximum shaking area respect to the epicentre, slightly altering the circular symmetry of the PGA distribution. Figure 15 shows the PGA map obtained for the November 1 mainshock. In this case, the area with PGA values greater then 100 gal (about 30 square kilometres) is located over the source.

Table 8. Source parameters adopted for simulation of the October 31 and November 1, 2002 Molise earthquakes, according to Basili and Vannoli [2005]. M_W : moment magnitude; M0 : seismic moment; Δu : average slip ; L and W : source dimentions; φ, δ and λ: strike, dip and rake; Z_{TOP} : top depth.

	M_W	$M_0[10^{17}Nm]$	Δu [cm]	LxW [km²]	$\varphi[°]$	$\delta[°]$	$\lambda[°]$	Z_{TOP} [km]
BV31	5.8	5.6	20	10.5 x 8.0	267	82	-157	12.0
BV01	5.7	4.0	18	9.4 x 8.0	261	86	-165	12.0
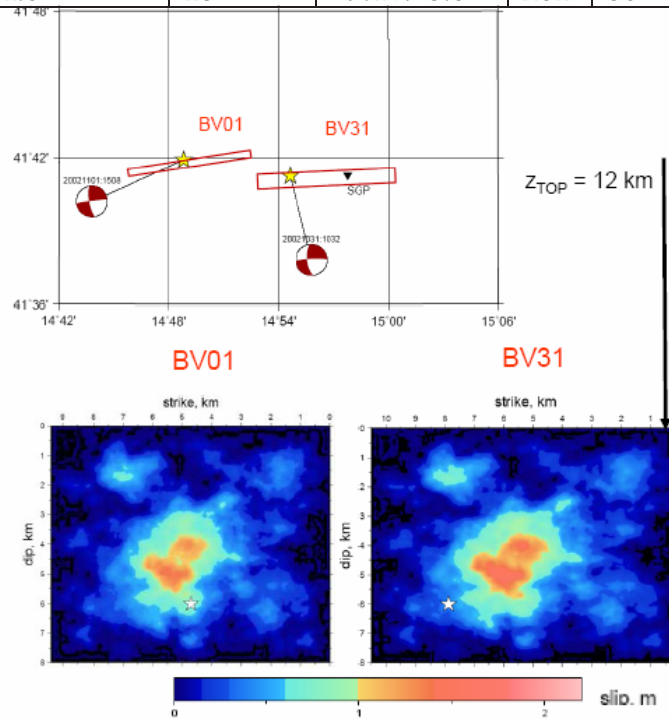
Figure 13. Fault surface projections (top) and slip distributions (bottom) adopted for the October 31, and November 1, 2002, Molise main shocks (models BV31 and BV01, respectively). Yellow stars mark surface projections of nucleation points corresponding to hypocenter locations (white stars on right panels). Corresponding focal mechanisms and the location of S.Giuliano di Puglia (SGP) are also shown.

In order to compare the ground shaking with macroseismic observations, the maximum PGA produced by the cumulative effect of the two main shocks in shown in Figure 16. The area characterized by PGA > 100 gal shows a good agreement with the isoseismal line of the VI degree MCS Intensity [see Galli and Molin, 2004, Figure 2]. Moreover, all sites located in the E-W direction over the surface projection of the two faults, experienced MCS intensities of VII degree, with the exception of San Giuliano di Puglia, located eastward, where I(MCS)=VIII-IX.

For both the October 31 and November 1 events, the attenuation of PGA with fault distance was estimated by averaging DSM simulations over all azimuths. Figure 17 shows the results in terms of mean value ±1std, up to 150 km. We can observe that the first event, characterized by the major directivity effect, produces a larger standard deviation. Directivity effects can also explain the higher mean values

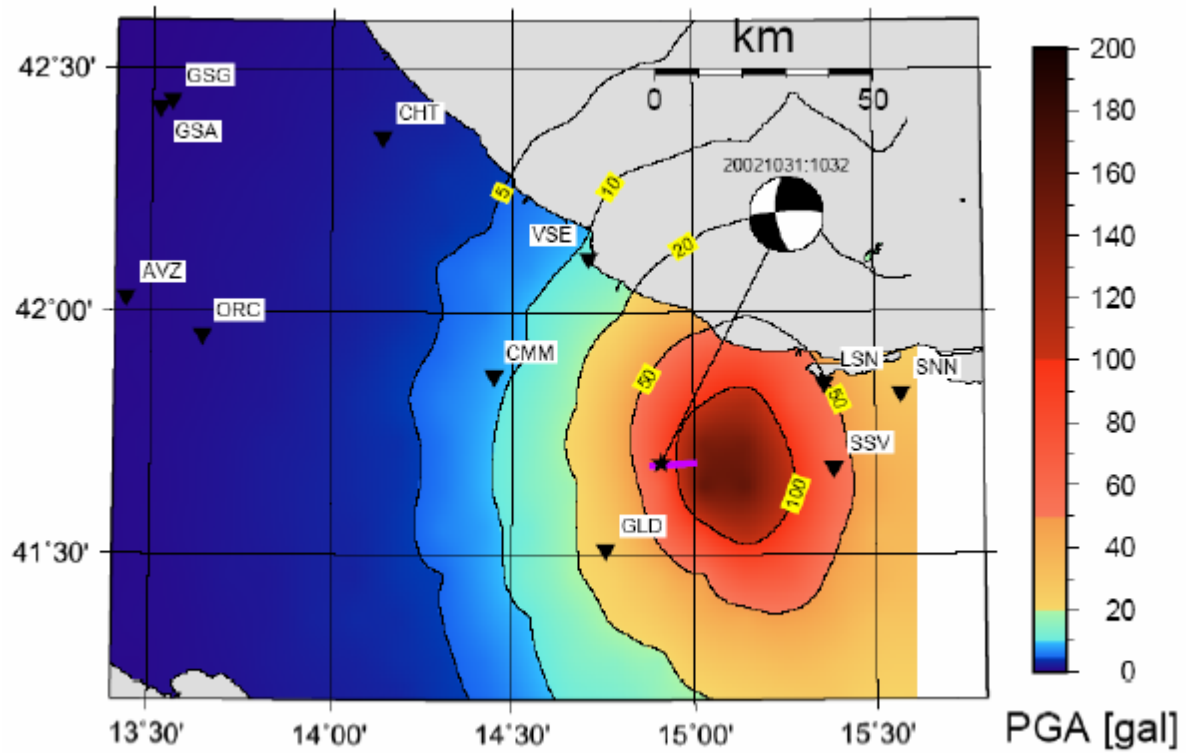obtained between 10 and 50 km fault distance.

Figure 14. PGA distribution (mean horizontal component) obtained by DSM with the BV31 model. Accelerometric stations recording the main events and the surface projection of the corresponding source (violet line) are also shown. A black star marks the position of the epicenter.
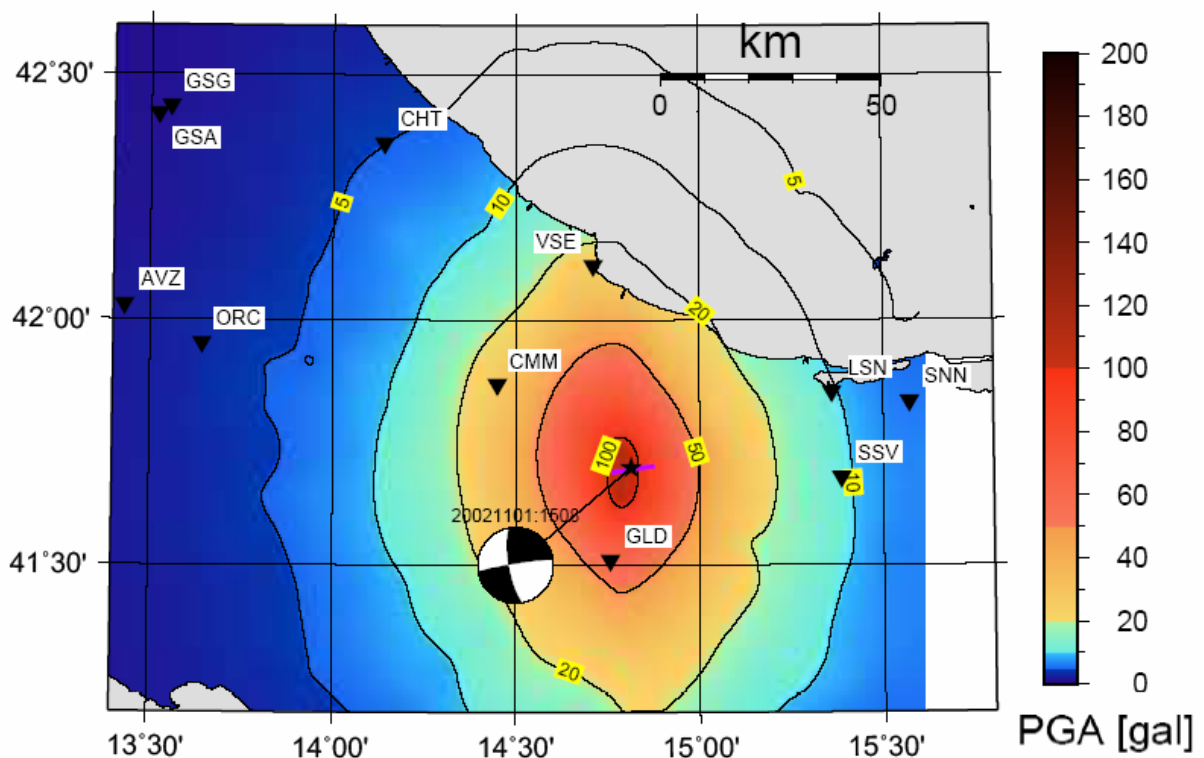
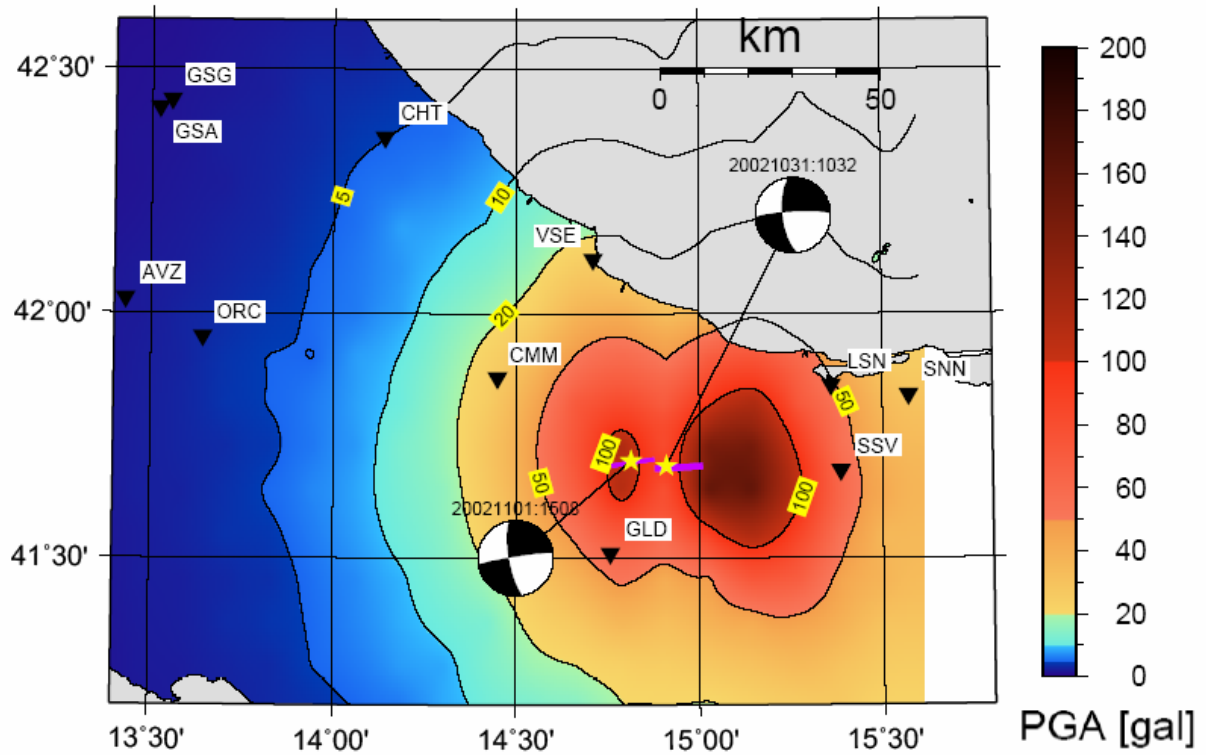**Figure 15. PGA distribution (mean horizontal component) obtained by DSM with the BV01 model. Symbols are as in Figure 14.**

Figure 16. PGA distribution (mean horizontal component) obtained by DSM produced by the cumulative effects of the October 31 and November 1 main shocks. Symbols are as in Figure 14.
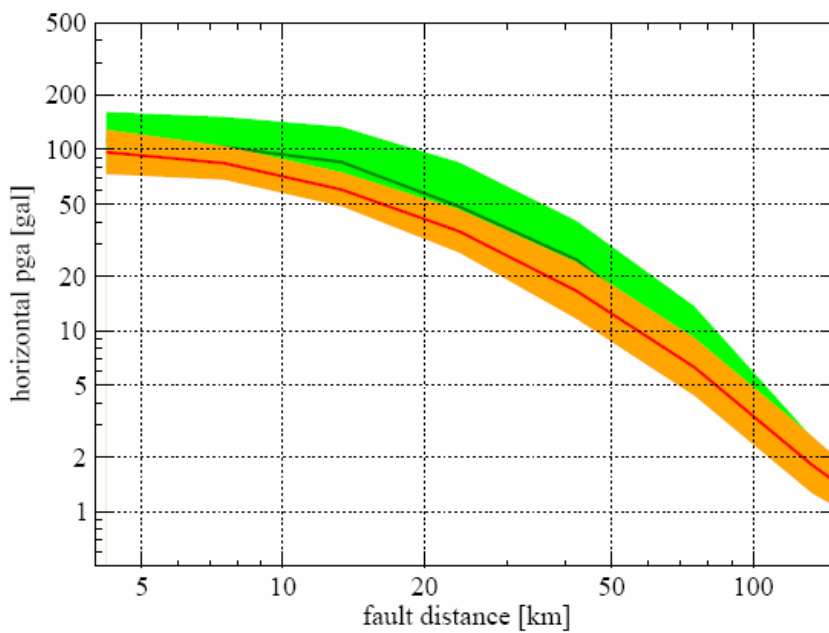
Figure 17. Mean horizontal component of the PGA obtained with BV31 and BV01 models (green and red curves, respectively). Shadow areas indicate PGA values in a range of ±1std from the mean.

4.4. Level II: HIC scenarios

Bedrock simulation has been performed for BV31 and BV01 models (Table 8) using the HIC method for receivers located at Ripabottoni (RPB), Bonefro (BNF), Santa Croce di Magliano (SCM), Colletorto (CLT) and San Giuliano di Puglia (SGIA; SGIB). Figure 18 shows the location of receivers and the surface projection of the employed source models.
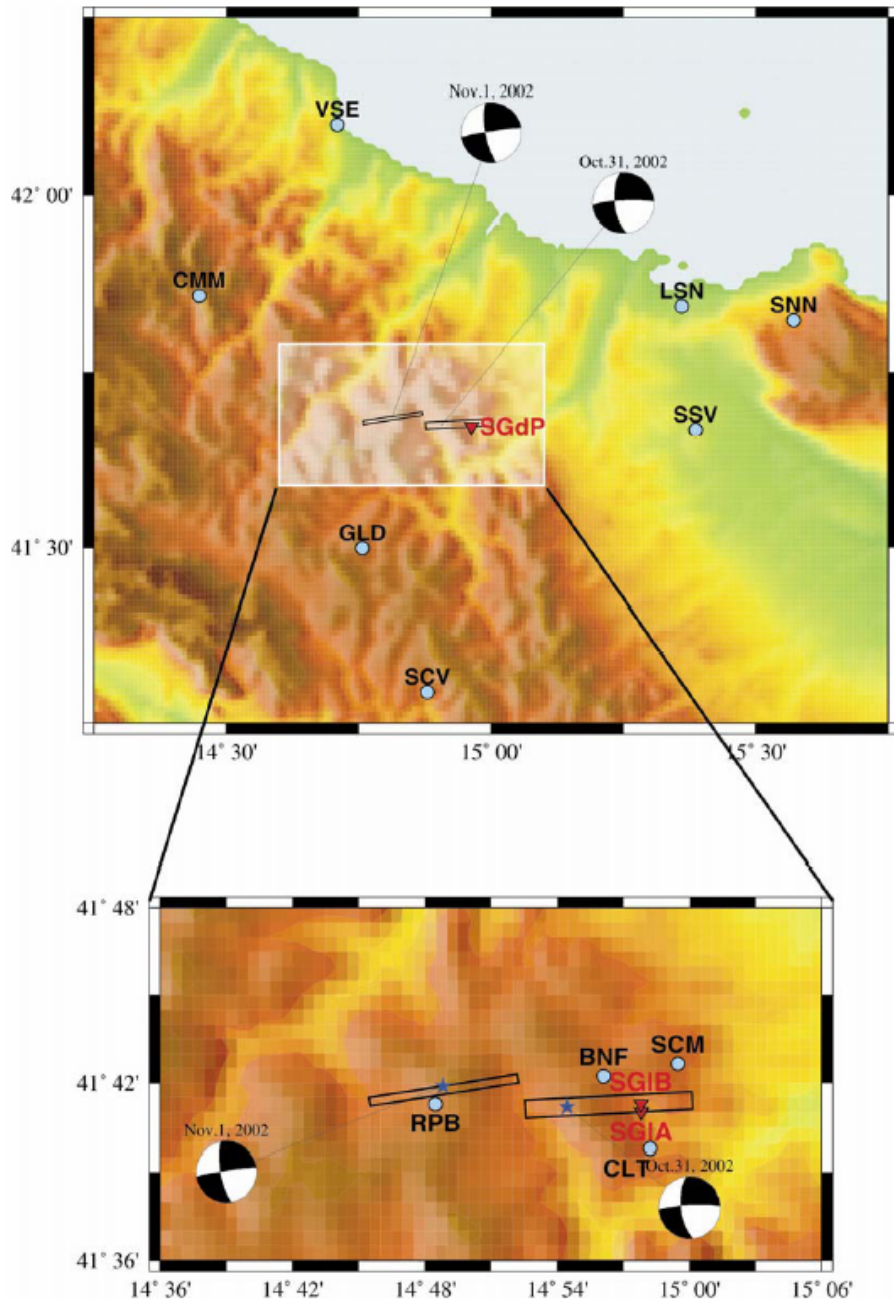

Figure 18. Surface projections and focal mechanisms of the fault models suggested by Basili and Vannoli [2005] for the October 31 and November 1, 2002 Molise earthquakes (lower panel). Locations of receivers RPB (Ripabottoni), BNF (Bonefro), SCM (Santa Croce di Magliano), CLT (Colletorto) and San Giuliano di Puglia (SGIA; SGIB) are also shown. Locations of the nearby accelerometric stations recording the main events are indicated in the upper panel (black labels).

As explained above, the HIC source model is composed of individual overlapping subsources distributed randomly along the fault, being suitable for both integral and composite source descriptions. Contrary to the integral k-squared approach, chaotic small-scale behavior is involved. It results in a more realistic directivity effect. Contrary to the composite approach, the model is better constrained for low-frequency calculation, e.g., for slip inversions (no artificial low-frequency filtering is necessary). The combination of the integral and composite approaches is numerically efficient with respect to the purely integral one. In this way, the method can provide input seismic motion in broad frequency range, starting practically at 0 Hz and extending to any frequency, 10 Hz in our case. Note that the spatial wavelength (or, alternativelly, frequency) dividing these two source representations is, in general, a subject of choice. In this case, we choose value of 1 Hz, which is commonly used value because the slip inversions that utilize integral approach are able to invert (describe) the data only up to 1 Hz.

Generally speaking, the HIC model has been tested previously on, e.g., the 1999 Athens, 1997 Kagoshima, or 1980 Irpinia earthquakes. Our modeling results for particular case of the Athens earthquake show that the hybrid approach predicts directivity in correspondence with observation (attenuation relations) in terms of the PGA scatter. The second example, the 1997 Kagoshima earthquake, shows that, despite the neglected site-effects, the model reproduces the complexity of measured velocity waveforms relatively well. As regards the Irpinia earthquake, the HIC model provided nice fit with the observed accelerometric records.

In the present computation, the main characteristics of the earthquake models are exactly the same as explained in the previous section. In particular, the subsources are distributed in such a way that the final slip distribution is that presented in Figure 13.

The separation of the computation into two parts allows different techniques to be used in computing Green's function in both frequency ranges. In the present calculations, we use DWN method, providing exact complete wavefield in the whole frequency range for 1D medium characterized by homogeneous layers (see Table 6).

In this way, the HIC than provides 3 component input motion, reproducing entire time series and not only the strong motion phase, albeit in the frame of the employed 1D crust model.

The resulting seismograms are shown in Figure 19 and Figure 20, for both earthquakes. Note the similar amplitudes at different components for each station. This is due to suppressed radiation pattern at high frequencies as discussed in §3.

As regard to receivers SGIA and SGIB, both located at S.Giuliano di Puglia, we can also note the strong similarity of the entire time series, due to the short inter-station distance (< 500 m).
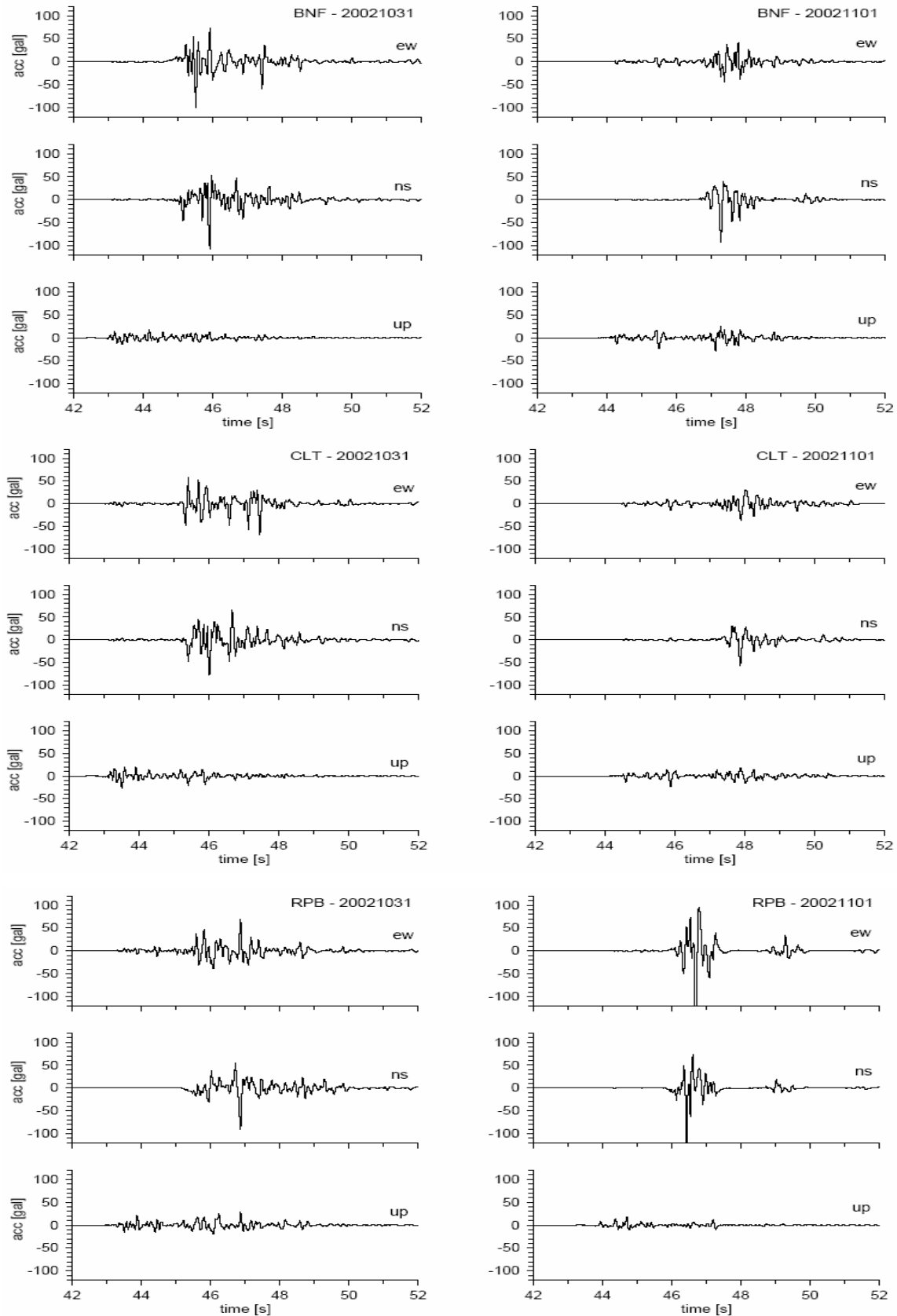
Figure 19. Acceleration time series obtained by HIC method at receivers BNF, CLT and RPB for the October 31 and November 1, 2002 events (left and right panels, respectively).
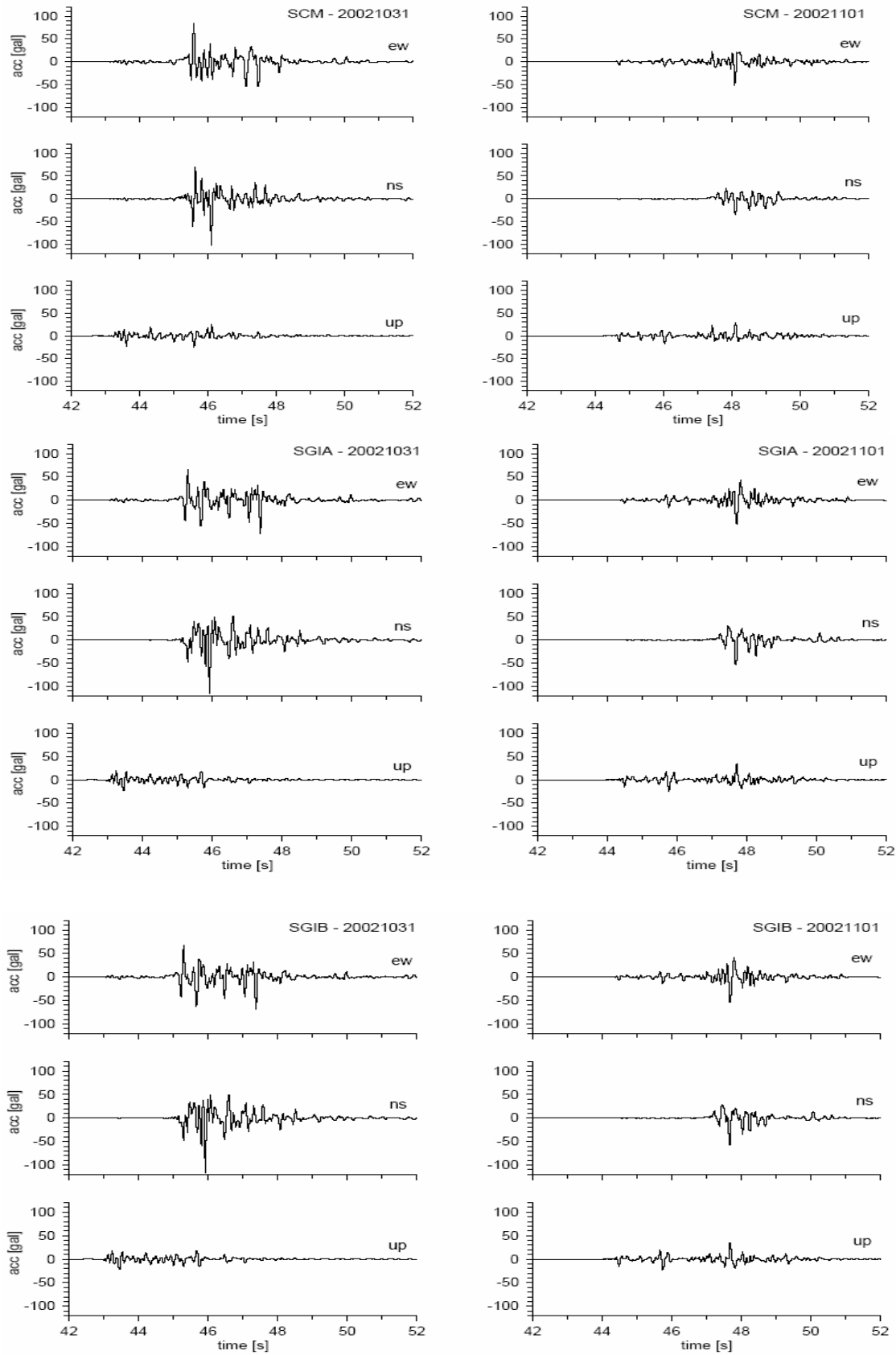
Figure 20. Same as Figure 19 but for receivers SCM, SGIA and SGIB.

4.5. Scenarios comparison

In order to validate the input motion to be used in the epicentral area for site effect modelling, scenarios of different levels have been compared in terms of peak values, spectral content and acceleration time series.

Figures 12, 17, 19 and 20 show that, in the epicentral area the bedrock shaking scenarios obtained by A95 (level 0), DSM (level I) and HIC (level II) produce peak accelerations around 100 gal.

A comparison between recorded and synthetic accelerations can be performed at longer distances. In particular, the frequency content of the time series produced by HIC and DSM was compared in terms of Amplitude Fourier Spectrum for different stations up to 50 km epicentral distance (Figure 21). Except for S.Giuliano di Puglia (SGI), the selected receivers correspond to accelerometric stations located both eastward (SSV) and westward (CMM and GLD) to the source. Due to their particular location, especially CMM and SSV are relevant for comparison of results obtained by DSM and HIC. Considering that, according to the hypothesized rupture model, SSV and CMM experience forward and backward directivity, respectively, from Figure 21 we can note that the spectral levels produced by HIC are much less sensitive to directivity effects than corresponding spectral levels obtained by DSM.

Acceleration spectra obtained at shorter distances with these two methods are more comparable, and it is worth mentioning that DSM spectra simulated at GLD are also well comparable with data (see Figure 11 and Table 7). At SGI (inside the surface projection of the fault), the spectral content of the ground motion simulated by HIC and DSM is practically equivalent, on condition that the frequency band 0.5-10 Hz is considered.
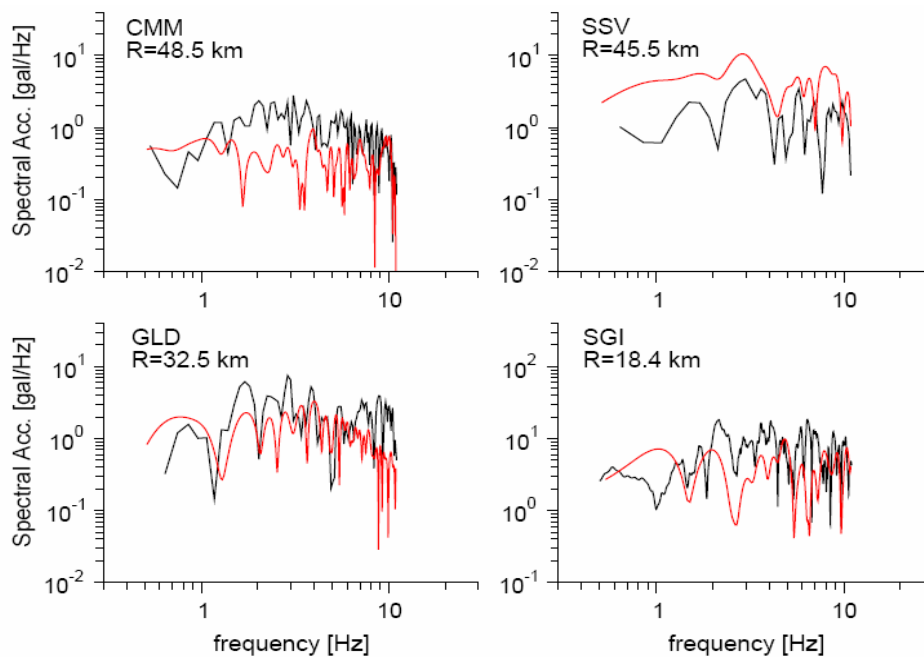

Figure 21. Simulated acceleration Fourier spectra at stations CMM, SSV, GLD and SGI, obtained by DSM and HIC method (red and black lines, respectively). Synthetic data refer to the October 31, 2002 main shock (NS component).

Acceleration time series obtained with HIC method and DSM in the epicentral area ($f_d < 5$ km) are compared to each other in Figures 22, 23, 24. The bedrock ground motion was computed at the 5 abovementioned municipalities in order to provide the best input motion for site effect modelling. After low –pass filtering below 11 Hz, DSM time series are generally comparable with HIC synthetics. Corresponding horizontal components show similar amplitude and frequency content, even if the two methods still show a different sensitivity to directivity effects (see receivers RPB and CLT, as an example).

The ground motion obtained by HIC, however, shows a higher level of complexity and longer durations, as a consequence of the more detailed modeling of both source and propagation effects. This is especially evident at sites experiencing forward directivity, where DSM simulations show particularly short durations and large amplitudes (see CLT, as an example).
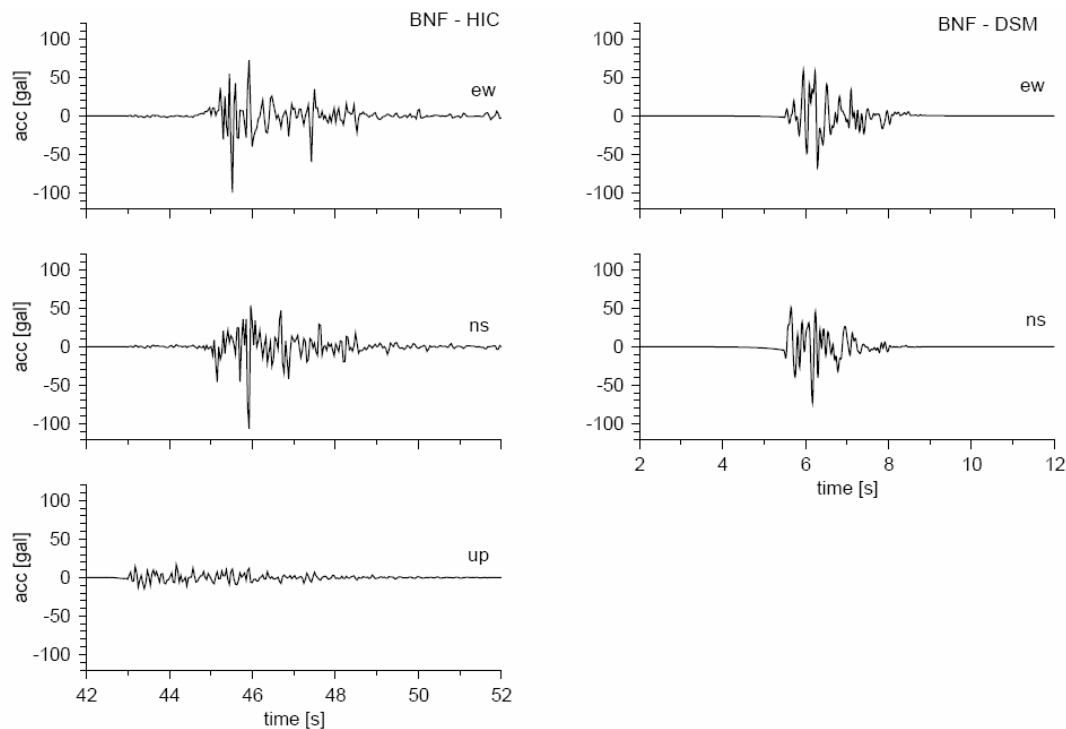

Figure 22. Acceleration time series simulated by HIC (left panels) and DSM (right panels) for the October 31, 2002 Molise earthquake (station BNF). For comparison purposes, DSM synthetics have been low-pass filtered at 11 Hz.
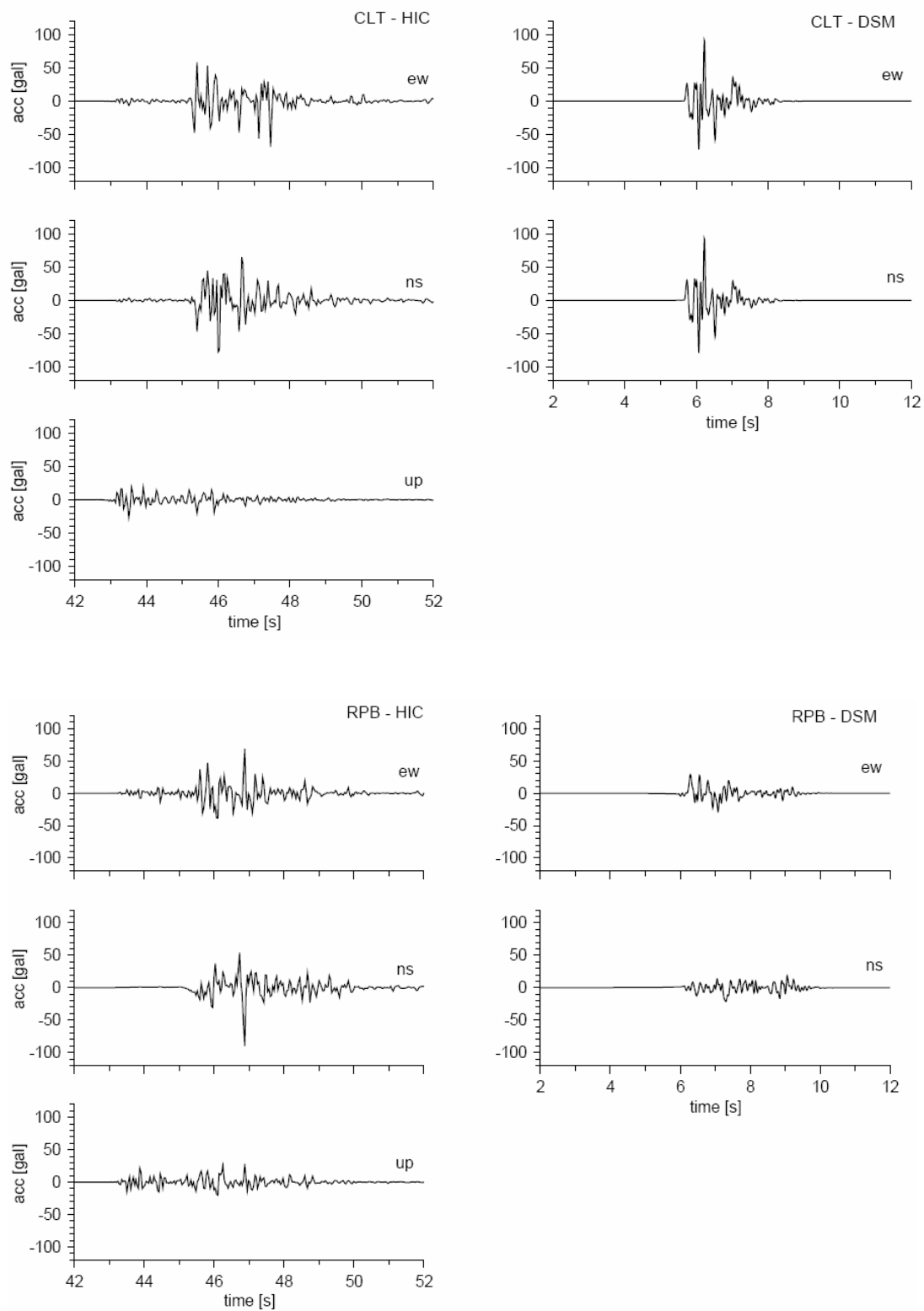
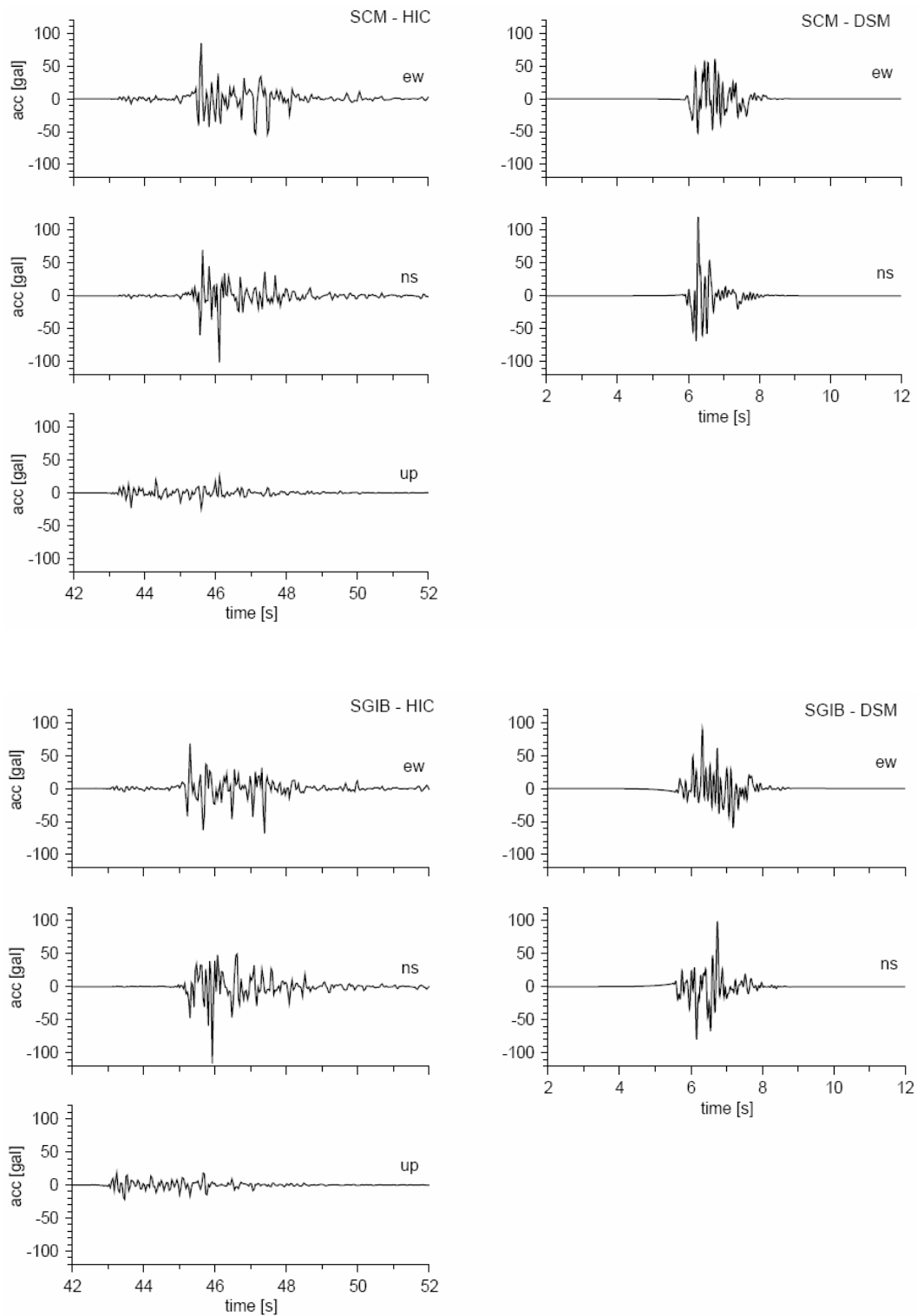**Figure 23. Same as Figure 22, but for stations CLT and RPB.**

Figure 24. Same as Figure 22, but for stations SCM and S.Giuliano di Puglia (SGIB).

5.   CONCLUSIONS

Notwithstanding the complexity of the Molise area as regard to both seismogenic source definition and attenuation properties of the crust, the comparison of results obtained by different simulation methods allows defining a reliable bedrock input motion for site effect modeling in the epicentral area.

The seismogenic sources of the October 31 and November 1, 2002 main events were selected based on comparison of observed and simulated acceleration spectra at nearby stations (hypocentral distance < 60 km). To that purpose we try to explain the different level of shaking observed at eastward and westward stations during the first mainshock as a directivity effect and simulated the rupture propagation on the hypothesized fault by the DSM. The sensitivity of this method in reproducing the high frequency directivity effects, allowed us to select the source model showing the best fit with both recorded spectra and peak values. At this stage, attenuation properties were introduced by a spectral attenuation model specifically developed for the area, using seismometric and accelerometric data recorded during the first month of seismic activity.

In order to define the near source input motion we employed the more advanced method, HIC, due to its ability in capturing many detailed features of the ground motion. Contrarily to DSM, the HIC method allows computing the three components of the acceleration time series in broad frequency range, starting practically at 0 Hz and extending to any frequency, 10 Hz in our case. It is known that the main disadvantage of a sophisticated simulation technique consists in a high dependence on input parameters. We thus compared the HIC time series (scenarios of level II) with results obtained by DSM (scenarios of level I) and GMPE (scenarios of level 0).

Such comparison shows that, up to about 30 km hypocentral distance, DSM and HIC method provide comparable acceleration time series in terms of amplitude and frequency content (between 1 and 10 Hz). Peak values are also comparable up to 50 km fault distance. Moreover, at these distances all the adopted methods provide peak accelerations practically compatible with the large dispersion of the observed data.

In the near source, synthetic peaks provided by DSM and HIC are also comparable with the depth-controlled GMPE suggested by Ambraseys [1995] for the European area. In this range of distances, sophisticated simulations computed by HIC method (scenarios of level II) are thus comparable with results of both scenarios of level I and 0. Therefore, in order to provide the input motion for site effect modelling, we suggest to select the input coming from the more advanced method employed at this stage of the project, because of its ability in capturing both durations and low frequency components of the earthquake ground motion.

BIBLIOGRAPHY

Abrahamson N. A., Youngs R. R. (1992). A stable algorithm for regression analyses using the random effects model, *Bull Seism. Soc. Am.*, **82**, 505-510

Ambraseys, N.N. (1995). The prediction of earthquake peak ground acceleration in Europe, *Earthquake Engng. Struct. Dyn.*, **24**, 467-490.

Anderson, J.G., Hough, S. (1984), A model for the shape of Fourier amplitude spectrum of acceleration at high frequencies, *Bull. Seism. Soc. Am.*, **74**, 1969-1994.

Andrews, D. J. (1980), A stochastic fault model, 1. Static case, *J.Geophys. Res.*, **85**, 3867-3877.

Bakun W. H., Joyner W. B. (1984), The Ml scale in central California, Bull. Seism. Soc. Am., 74, 1827–1843

Basili, R., and Vannoli, P. (2005). Source ITGG052 *San Giuliano di Puglia* and Source ITGG053 *Ripabottoni*. In: DISS Working Group, Database of Individual Seismogenic Sources (DISS), Version 3.0.1: A compilation of potential sources for earthquakes larger than M 5.5 in Italy and surrounding areas. http://www.ingv.it/DISS/ - Istituto Nazionale di Geofisica e Vulcanologia.

Bernard, P. and Madariaga, R. (1984), A new asymptotic method for the modeling of near field accelerograms, *Bull. Seism. Soc. Am.*, **74**, 539-558.

Boore, D. M. (2003), Simulation of ground motion using the stochastic method, *Pure Appl. Geophys.,* **160**, 635-676.

Bouchon, M. (1981),   A simple method to calculate Green's functions for elastic layered media, *Bull. Seism. Soc. Am.*, **71**, 959-971.

Bindi D., Luzi L., Pacor F., Franceschina G., Castro R. R. (2006). Ground motion predictions from empirical attenuation relationships versus recorded data: the case of the 1997-98 Umbria-Marche (Central Italy) strong motion data-set, *Bull Seism. Soc. Am.*, 96, **3**, 984–1002.

Brune, J. (1970). Tectonic stress and the spectra of seismic shear waves from earthquakes, *J. Geophys. Res.*, **75**, 4997-5009 (correction, *J. Geophys. Res.*, **76**, 5002).

Castro, R. R., J. G. Anderson, and S. K. Singh (1990). Site response, attenuation and source spectra of S waves along the Guerrero, Mexico, subduction zone, *Bull. Seism. Soc. Am*, **80**, 1481-1503.

Chiarabba C., DeGori P., Chiaraluce L., Bordoni P., Cattaneo M., Demartin C., Frepoli A., Michelini A., Monachesi G., Moretti M., Augliera P., D'Alema E., Frapiccini M., Gassi A., Marzorati S., Molise Working Group (INOGS, Dipteris Unige) (2005). Mainshocks and aftershocks of the 2002 Molise seismic sequence, southern Italy, *J. Seismol.*, **9**, 487-494.

Dipartimento della Protezione Civile - Ufficio Servizio Sismico Nazionale - Servizio Sistemi di Monitoraggio (2004). The Strong Motion Records of Molise Sequence

(October 2002 - December 2003), CD-ROM, Rome.

Galli, P. and Molin, D. (2004), Macroseismic Survey of the 2002 Molise, Italy, Earthquake and Historical Seismicity of San Giuliano di Puglia, *Earthquake Spectra*, **20-S1**, S39-S52.

Gallovic, F. and Brokesova, J. (2007), Hybrid k-squared Source Model for Strong Ground Motion Simulations: Introduction, *Physics .Earth. Planet. Int.,* **160**, 34-50.

Maffei, J. and Bazzurro, P. (2004), The 2002 Molise, Italy, Earthquake, *Earthquake Spectra,* **20-S1**, S1-S22.

Nuti, C., Santini, S. and Vanzi, I. (2004), Damage, Vulnerability and Retrofitting Strategies for the Molise Hospital System Following the 2002 Molise, Italy, Earthquake, *Earthquake Spectra,* **20-S1**, S285-S299.

Pacor, F., Cultrera, G., Mendez, A. and Cocco, M. (2005), Finite Fault Modeling of Strong Motion Using a Hybrid Deterministic-Stochastic Approach, *Bull. Seism. Soc. Am.*, **95**, 225-240.

Richter, C. F. (1935). An instrumental earthquake magnitude scale. *Bull. Seism. Soc. Am.*, **25**, 1-32.

Sabetta, F. and A. Pugliese (1996), Estimation of response spectra and simulation of nonstationary earthquake ground motion, *Bull. Seism. Soc. Am.*, **86**, 337-352.

Spudich, P. and Frazer, L.N. (1984), Use of ray theory to calculate high frequency radiation from earthquake sources having spatially variable rupture velocity and stress drop, *Bull. Seism. Soc. Am.*, **74**, 2061-2082.

Valensise, G., Pantosti, D. and Basili, R. (2004), Seismology and Tectonic Setting of the 2002 Molise, Italy, Earthquake, *Earthquake Spectra,* **20-S1**, S23-S37.

Vallée, M. and Di Luccio, F. (2005), Source analysis of the 2002 Molise, southern Italy, twin earthquakes (10/31 and 11/01), *Geophys. Res. Lett.,* **32**, L12309.

Wells, D.L. and Coppersmith, K.J. (1994), New Empirical Relationships among Magnitude, Rupture Length, Rupture Width, Rupture Area, and Surface Displacement, *Bull. Seism. Soc. Am.*, **84**, 974-1002.

Zeng, Y., Anderson, J. G. and Yu, G. (1994), A composite source model for computing realistic synthetic strong ground motions, *Geophys. Res. Lett.*, **21**, 725-728.